ENN Encyclopedia of Nanoscience and Nanotechnology
www.aspbs.com/enn

Nanoscale Heat Transfer

G. Chen, D. Borca-Tasciuc, R. G. Yang

Massachusetts Institute of Technology, Cambridge, Massachusetts, USA

CONTENTS

1. INTRODUCTION

Heat transfer at nanoscale is of importance for many nanotechnology applications [1, 2]. There are typically two types of problems. One is the management of heat generated in nanoscale devices to maintain the functionality and reliability of these devices. The other is to utilize nanostructures to manipulate the heat flow and energy conversion. Examples of the thermal management of nanodevices are the heating issues in integrated circuits [3] and in semiconductor lasers [4]. Examples in the manipulation of heat flow and energy conversion include nanostructures for thermoelectric energy conversion [5, 6], thermophotovoltaic power generation [7], and data storage [8].

Heat transfer at nanoscale may differ significantly from that in macro- and microscales. With device or structure characteristic length scales becoming comparable to the mean free path and wavelength of heat carriers (electrons, photons, phonons, and molecules), classical laws are no longer valid and new approaches must be taken to predict heat transfer at nanoscale [9, 10]. Well-known examples are the failure of Fourier law to predict the thermal conductivity of composite nanostructures such as superlattices [11, 12] and the failure of the Stefan–Boltzmann law in predicting radiation heat transfer across small gaps [13, 14]. Although much has been done in this area recently, there is still an immediate need for a better understanding of thermal phenomena in nanostructures. In addition, learning to control and manipulate heat carriers in small structures may open new paths for discovery of innovative applications.

In this chapter, we review the status and progress of theoretical and experimental investigations of thermal transport phenomena in nanostructures. In Section 2, we discuss different regimes of nanoscale heat transfer and various nanoscale heat transfer phenomena. Section 3 gives a few examples that illustrate the impacts of nanoscale thermal phenomena on modern technologies. Section 4 describes several experimental techniques developed for thermal characterization of nanostructures. Section 5 summarizes modeling tools for nanoscale heat transfer, followed by a summary of this chapter.

2. FUNDAMENTALS OF HEAT TRANSPORT AT NANOSCALE

Macroscale heat transfer is often divided into three modes: conduction, convection, and radiation [15]. Heat transfer problems are solved based on the conservation laws (mass, momentum, and energy) in combination with the constitutive equations between heat flux and temperature (or temperature gradient), for example, the Fourier law of heat conduction and the Stefan–Boltzmann law for blackbody thermal radiation,

$$q = -k\nabla T \quad \text{(Fourier law)}$$
$$q = \sigma T^4 \quad \text{(Stefan–Boltzmann law)} \tag{1}$$

where k is the thermal conductivity and σ is the Stefan–Boltzmann constant (5.67×10^{-8} W/m^2 K^4). Some distinct characteristics of heat transfer at macroscale are:

1. The Fourier law is a diffusion equation while thermal radiation between two objects separated by a nonabsorbing (or weakly absorbing) medium is ballistic.
2. Thermal conductivity is a material property which may depend on the detailed microstructure of the material but is independent of the size of the material.
3. The maximum thermal radiation heat transfer between any objects is limited by the blackbody radiation.
4. In convection, the fluid in contact with the solid assumes the same velocity and temperature as the solid at the point of contact, the so-called no-slip condition.

For heat transfer in nanostructures, some of these characteristics for macroscale heat transfer disappear. For example, heat conduction can be ballistic and similar to thermal

ISBN: 1-58883-063-2/$35.00

Encyclopedia of Nanoscience and Nanotechnology
Edited by H. S. Nalwa
Volume 7: Pages (429–459)

radiation; thermal conductivity is no longer a material property; thermal radiation can be larger than the blackbody radiation; and the slip of molecules at fluid–solid interface must be considered. To understand why and when these happen, one needs to examine carefully the microscopic pictures of the heat carriers including molecules, electrons, photons, phonons (quantized lattice vibrations), or their hybrid states such as plasmons and phonon–polaritons [16, 17]. Table 1 shows some elementary properties of electrons, phonons, photons, and molecules. We will start with a discussion of the characteristic lengths of some of these energy carriers. From such a discussion, different transport regimes can be distinguished [4, 9, 10].

2.1. Characteristic Lengths and Heat Transfer Regimes

From quantum mechanics, the energy carriers have both wave and particle characteristics. At macroscale, wave phenomena such as interference and tunneling usually do not appear and we often treat the energy carriers as particles. At nanoscale, however, wave effects become important and even dominant in some cases. A key question is when one should start to consider the wave characteristics. There are a few important characteristic length and time scales that determine the answer to this question, including the mean free path, the phase coherence length, the wavelength, and the thermal (de Broglie) wavelength, which we will explain.

The mean free path is the average distance that energy carriers travel between successive collisions, such as the phonon–phonon collision in a dielectric material and the electron–phonon collision in a conductor or semiconductor. The corresponding average time between successive collisions is the relaxation time. Direct calculation of the mean free path is generally difficult, particularly for electron and phonon transports in solid. The kinetic theories and experimental conductivity data are often used to estimate the mean free path. For example, the thermal conductivities of gases, metals, and semiconductors or dielectrics can be expressed as [16–19]

$$k = \frac{1}{3} C v^2 \tau = \frac{1}{3} C v \Lambda \qquad \text{(gases)} \tag{2}$$

$$k = \frac{\pi^2 n \kappa_B^2 T}{m v_F} \Lambda \qquad \text{(electrons in metals)} \tag{3}$$

$$k = \frac{1}{3} \int_0^{\omega_{\max}} C_\omega v_\omega^2 \tau_\omega \, d\omega = \frac{\Lambda}{3} \int_0^{\omega_{\max}} C_\omega v_\omega \, d\omega \qquad \text{(phonons)} \tag{4}$$

where C is the volumetric specific heat (i.e., the specific heat per unit volume), τ is the relaxation time, v is the velocity of carriers, m is the electron mass, n is the electron number density, and v_F is the electron velocity at the Fermi surface. The integration in Eq. (4) is over all the phonon frequency and correspondingly, C_ω, v_ω, and τ_ω are the volumetric specific heat, the velocity, and the relaxation time at each frequency, respectively. This distinction is necessary because phonons are highly dispersive. If Eq. (2) is used to estimate the phonon mean free path, using the measured specific heat and the speed of sound, the mean free path can be an order of magnitude lower than that based on Eq. (4) [20–22]. In Figure 1, we show the mean free path in representative media. Also shown in this figure is an example of the phonon mean free path in silicon estimated based on Eq. (2), using the reported data on specific heat and the speed of sound, which is an order of magnitude shorter than that estimated from considering the phonon dispersion.

The phase of a wave can be destroyed during collision, which is typically the case in inelastic scattering processes, such as the electron–phonon collision and phonon–phonon collision. An inelastic scattering process is the one that involves the energy exchange between carriers. If the phase destroying scattering process occurs frequently inside the medium, the wave characteristic of carriers can be ignored and the transport falls into the diffusion regime. The measure for the phase destroying scattering events is called the phase coherence length and, for electron transport, the Thouless length [23]. Not all the scattering processes, however, destroy the phase. Elastic scattering processes such as scattering of photons by particulates and the scattering of electrons by impurities do not destroy phase. Thus, the phase coherence length is usually longer than the mean free path but is not much longer, particularly at room temperatures for electrons and phonons. Therefore we can treat them as having the same order of magnitude.

Thus, one necessary condition for the inclusion of the wave effects is that the mean free path should be comparable to or larger than the structure characteristic length, such as the thickness of a film or the diameter of a wire. This condition, however, is not sufficient for actually observing the wave effects because of three additional factors, (1) the interface scattering processes, (2) the wavelength of the carriers, and (3) the spectrum of the carriers, as will be explained.

When the wave meets an interface, it will be scattered. The most familiar example is the reflection and refraction of optical waves [24]. Electron waves and phonon waves

Table 1. Basic characteristics of energy carriers.

	Electrons	Phonons	Photons	Molecules
Propagation media	in vacuum or media	in media	in vacuum or media	in vacuum or media
Statistics	Fermi–Dirac	Bose–Einstein	Bose–Einstein	Boltzman
Frequency	0–infinite	0–Debyte cutoff	0–infinite	0–infinite
Wavelength at 300 K (nm)	~10	~1	$\sim 10^5$	~0.1
Velocity at 300 K (m/s)	$\sim 10^6$	$\sim 10^3$	$\sim 10^8$	$\sim 10^2$

Source: Adapted with permission from [10], C. L. Tien and G. Chen, *Trans. ASME, J. Heat Transf.* 116, 779 (1994). © 1994, American Society of Mechanical Engineers.

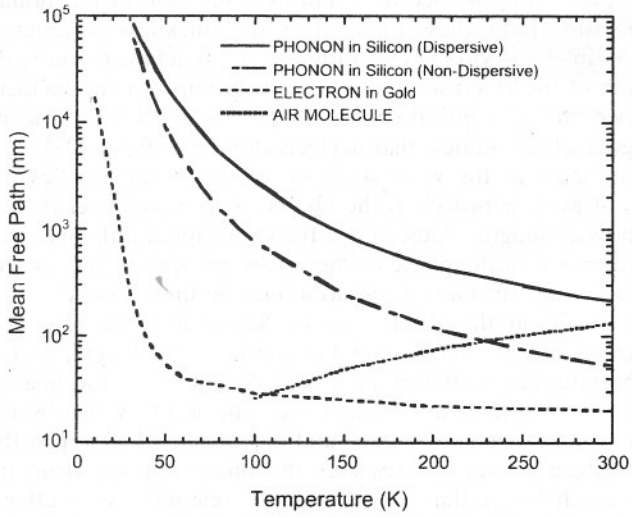

Figure 1. Mean free path for representative energy carriers.

have similar processes. For a flat interface, the phases and directions of the refracted and reflected waves are fixed relative to the incident waves. These processes thus do not destroy the phases. Periodic interface corrugations, such as surface gratings, are another example for which the incident and outgoing waves have clear fixed phase relations. Rough interfaces, however, are more complicated. If the detailed interface roughness structures are known and if the interface interaction is elastic, the directions of the reflected and refracted waves can in principle be determined from, for example, solving the Maxwell equations for photons and the Schrödinger equation for electrons and phonons. In reality, this is rarely possible and rough interface scattering is often assumed to diffuse (i.e., the reflected and transmitted waves are isotropically distributed into all directions). Often, the accompanying assumption is that the relationship between the phases of the reflected, transmitted, and incident wave is lost (i.e., the scattering is phase randomizing). Such an assumption cannot be justified easily but appears to be true in many transport processes, particularly for phonons and photons. Clearly, in addition to elastic scattering, inelastic scattering can be also strong at the interfaces and such scattering processes are phase breaking. Thus, the interface scattering can be approximated as phase breaking if the interface is rough and as phase preserving if it is smooth. Whether an interface is rough or smooth depends on the average roughness, δ, compared to the wavelength λ. For example, an approximate expression for the fraction of specular scattered phonons at an interface is [19]

$$p = \exp\left(-\frac{16\pi^3\delta^2}{\lambda^2}\right) \tag{5}$$

From this expression, we can approximately take

$$\frac{\delta}{\lambda}\begin{cases} \gg 0.1 & \text{(Rough)} \\ \ll 0.1 & \text{(Smooth)} \end{cases} \tag{6}$$

Based on the previous discussion, if the interface scattering is diffuse, the wave aspects of energy carriers can be neglected. If the interface scattering processes preserve the phase relations, coherent waves may be established over the transport domain. Even under such situations, however, wave effects may still be unobservable. There are two additional factors that one should consider. One is the wavelength of the energy carriers and the other is the thermal spread in their wavelengths.

Heat transfer usually involves a wide spectrum of energy carriers, as summarized in Table 1. However, not all the energy carriers spanning such a wide range of wavelength contribute equally to the thermal transport. The actual probability of excitation for a specific quantum mechanical state depends on the energy of the state and the temperature of the object as governed by the Fermi–Dirac distribution for electrons and the Bose–Einstein distribution for phonons and photons. The blackbody radiation is a well-known example, with the emissive power peaks at

$$\lambda T = 2898\ \mu\text{m}\cdot\text{K} \tag{7}$$

which is known as the Wien displacement law [25].

We can estimate the order of magnitude of the average wavelength of the energy carriers, λ_t, by assuming the average energy of one quantum state is $\kappa_B T/2$, where $\kappa_B (= 1.38 \times 10^{-23}$ J/K) is the Boltzmann constant and calculating the corresponding wavelength from the de Broglie relation, $\lambda = h/p$, for material waves or from the Planck relation $E = h\nu$ for phonons and photons, where $h (= 6.6 \times 10^{-34}$ J·s) is the Planck constant, p is the momentum, and ν is the frequency. This leads to

$$\lambda_t = \frac{h}{\sqrt{3m\kappa_B T}} \qquad \text{(for electrons or molecules)} \tag{8}$$

$$\lambda_t = \frac{2h\nu}{\kappa_B T} \qquad \text{(for photons and phonons)} \tag{9}$$

where v is the speed of carriers. Equations (8) and (9) are also close to the thermal de Broglie wavelength but, for accuracy, we will just call it the thermal wavelength. Figure 2 plots the wavelength as a function of temperature for these

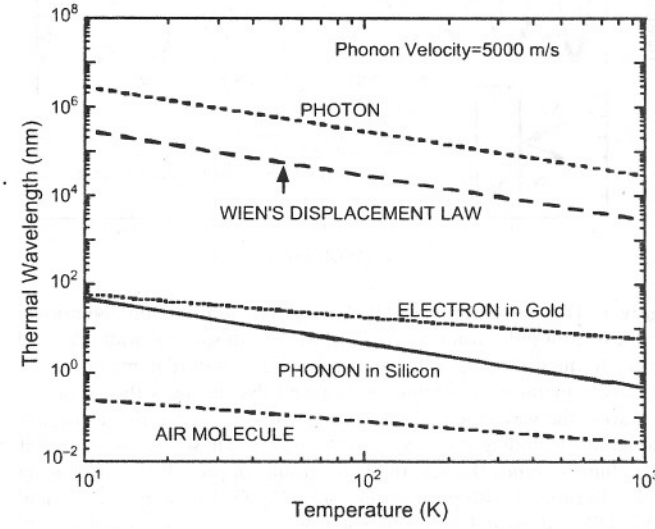

Figure 2. Thermal wavelength for representative energy carriers.

carriers with representative mass and velocity values. We also plotted the Wien displacement law. At room temperature, the wavelength orders of magnitudes are 1 Å for molecules, 10 Å for phonons, 100 Å for electrons, and 100 μm for photons.

In addition to the thermal wavelength, we should also consider the spread in energy and wavelength of the carriers. The superposition of waves forms wave packets that travel at the group velocity. In optics, the width of the wave packets is called the coherence length and is of the order of [24]

$$l_c \approx \frac{c}{\Delta\nu} \tag{10}$$

where c is the speed of light and $\Delta\nu$ is bandwidth of the radiation. This terminology will not be used here to avoid the confusion with the phase coherence length we discussed earlier. For thermal transport, the spread in thermal energy is also of the order of $\kappa_B T$. Thus, the wave packet width of the thermally excited energy carriers is of the same order of magnitude as the thermal wavelength, although a different definition can give some different results, particularly for thermal radiation [21, 26]. In the following, we will use the thermal wavelength as a measure of the wave packet size.

Because of the spread in the wavelengths of the energy carriers, the wave effects maybe smeared out and unobservable. The best example is the Young interference experiments of light passing through two slits. When the slit separation is small, interference is observable. In the opposite limit, the effect is unobservable. In this case, interference for each spectrum in the wave packet still occurs but is smeared out due to the superposition of the interference patterns of different wavelengths. In Figure 3, we show the optical transmittance of a film as a function of the nondimensional thickness (defined as the thickness parameter) obtained based on three different approaches: (1) integration of the electromagnetic wave solution over the incident spectrum, (2) optical coherence theory, and (3) ray tracing (geometrical optics) that neglects the wave effects [27]. One can see that the wave solution eventually approaches the ray-tracing approach as the film becomes much thicker than the wavelength. Thus, in the thick film limit, although consideration of the phase of the waves can lead to the correct end result, such a consideration may be unnecessary.

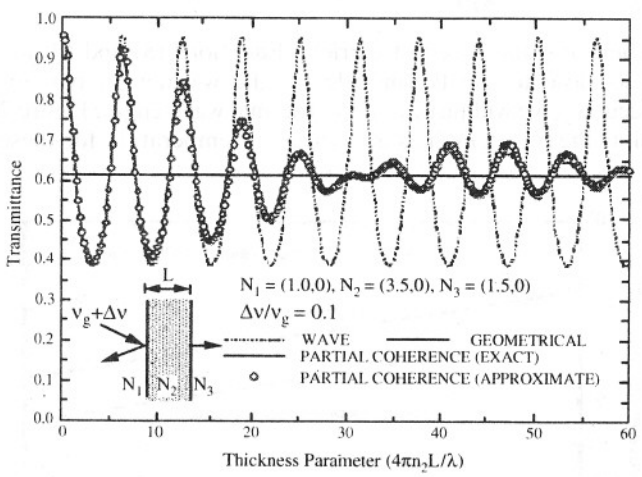

Figure 3. Transmittance of a film as a function of nondimensional thickness for a polychromatic incident wave with spectral width $\Delta\nu$ and central frequency at ν_g, calculated from three different methods, the ray tracing method (or geometrical optics) that neglects the phases of the waves, the wave method, and the partial coherence theory formulation, both including the phases of the waves. These results show that as the film becomes thicker, the wave results approach the ray tracing results. Reprinted with permission from [27], G. Chen and C. L. Tien, *Trans. ASME, J. Heat Transf.* 114, 636 (1992). © 1992, American Society of Mechanical Engineers.

Based on this discussion, we see that if the structure size is much smaller than the thermal wavelength, and if the interface scattering processes do not break the phases, the wave effects are distinct and one is likely to observe such effects as interference and diffraction. However, if the interface scattering preserves the phase but the structure is much larger than the thermal wavelength, wave effects can be obscured and not distinct. Under such conditions, as an approximation, some transport problems can be treated without considering the phase information of the energy carriers. We should emphasize, however, that this approximation is not always true. As an example of the failure of the previous approximation, we consider the acoustic wave transmission through a periodic thin film structure (i.e., a superlattice). The transmissivity was calculated with two methods, the acoustic wave transfer matrix method that includes the phases of the waves and the ray-tracing method that does not include the phase information [28]. The transmissivity is averaged thermally excited phonons incident from all allowable angles. Figure 4a and b shows the thermal conductance through a periodic superlattice, which is proportional to transmissivity. As the thickness of each layer increases, the thermal conductance approaches a constant as shown in Figure 4a. This occurs around 10 Å—the order of magnitude of the phonon thermal wavelength at room temperature. This constant thermal conductance, however, is different from that obtained with ray tracing, as shown in Figure 4b. As the number of layers in such a periodic structure increases, the figure shows a thermal conductance or transmissivity that asymptotically approaches zero as more layers are added. Clearly, in this case, ray tracing is not a good approximation to the wave approach.

Both Figure 3 and Figure 4 consider the wave propagation through thin film systems, but they lead to quite different conclusions (i.e., in the former case, the ray tracing approximation is valid while not for the latter case). We use wave packet propagation as shown in Figure 5 to explain the difference. A wave packet can experience multiple reflections in a film. In a single layer thick film (Fig. 5a), for example, the multiple reflection of a small wave packet does not overlap with itself. In a periodic structure, however, the same wave packets split at different interfaces have a chance of overlapping each other, as sketched in Figure 5b. Because of the overlapping of the same wave packets, there is always the wave interference effect, despite the fact that these effects are not reflected as periodic variations of the transmittance due to thermal averaging effects.

With the previous discussion, we can now divide the nanoscale heat transfer into several regimes as shown in Figure 6. The first demarcation line is the mean free path

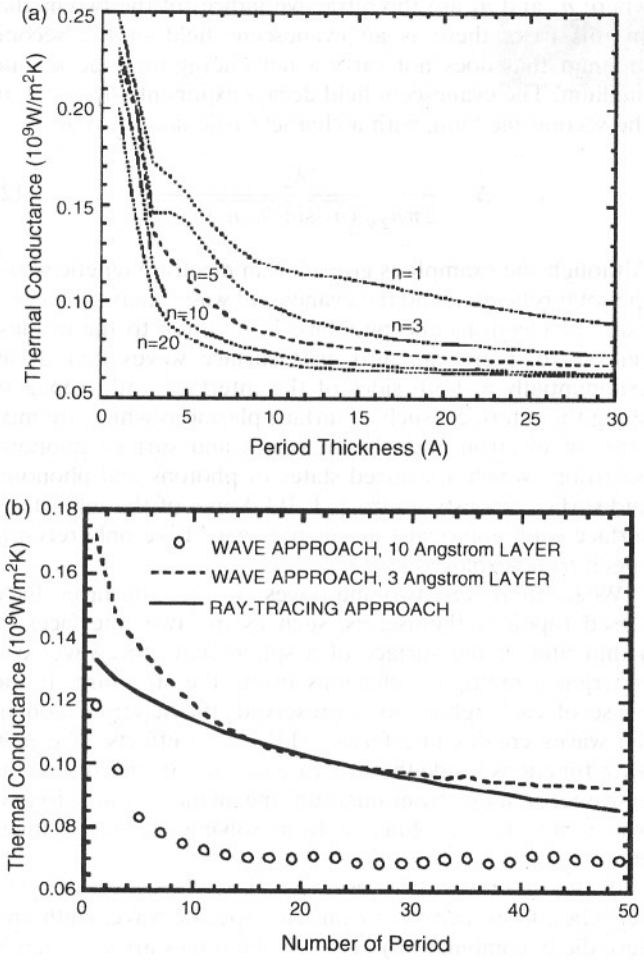

Figure 4. Thermal conductance based on calculation of acoustic waves through a periodic superlattice showing that the wave approach does not necessary lead to the same results as the ray tracing approach. Panel (a) shows that thermal conductance does not change when the layer thickness is larger than 20 Å, of the order of thermal wavelength. However, (b) shows that while the wave treatment leads to a nonzero conductance with increasing number of periods, ray tracing treatment leads to thermal conductance asymptotically approaching zero. Both calculations neglected internal scattering and assumed perfect interfaces. Reprinted with permission from [28], G. Chen, *Trans. ASME, J. Heat Transf.* 121, 945 (1999). © 1999, American Society of Mechanical Engineers.

(or phase coherence length) versus the characteristic structure size. Here, we emphasize that the mean free path and phase coherence length are values in bulk materials. Boundary effects will be discussed latter. If the structure is much larger than the mean free path, transport is a diffusion process (or drift-diffusion as for convection and electron transport under a driven current). When the structure is comparable to or smaller than the mean free path, size effects begin to appear and eventually become dominant. The actual numbers that demarcate different regimes are not to be considered accurate. For example, in rarefied gas dynamics, the continuum regime is assumed when $d/\Lambda > 100$ [29], while we used 10 in Figure 6. We further distinguish the size effects into the classical size effect regime and the quantum size effect regime, depending on whether the phase

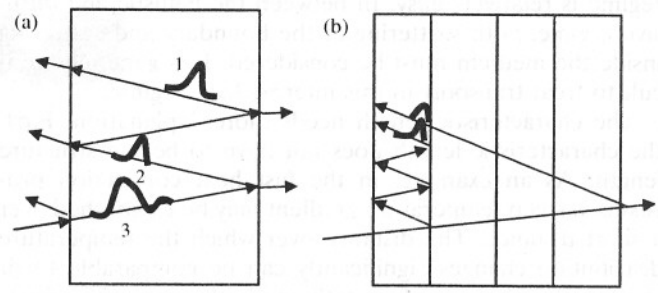

Figure 5. Traveling and interference of the same incident wave packet inside a film and a superlattice. (a) Inside a thick film, the same packet experiences multiple reflections and splitting at each reflection. When the film is thick, there is little chance that these split wave packets can overlap. The end results are that no interference beats can be observed and thus ray tracing can be used without considering the phase of the waves. (b) In a period structure, however, the same wave packets are split many times at different interfaces and it is possible a wave packet experiencing multiple reflections in one layer can overlap with that reflected into the same location from other layers. Because of this process, the ray tracing method will never lead to the same results as the wave optics even when each layer is very thick.

of the energy carriers needs to be considered. In addition to the classical and quantum size regimes, we sometimes also call these regimes particle and wave regimes or incoherent and coherent transport regimes, because it is not always necessary to treat the waves as quantized waves, such as the case for electromagnetic waves. In the classical size effects regime, one can ignore the phase of the energy carriers and trace their trajectories. Whether the transport is in the classical or quantum size effects regime depends on whether the interface scattering processes can maintain the phases of the waves. We used the terminology of interface phase-breaking scattering strength to distinguish the classical and quantum size effects regime rather than just the interface roughness, to emphasize that only complete phase breaking can justify neglecting phases associated with the carriers. In the quantum size regime, the phase information is important and must be considered. When the structure characteristic length is much smaller than the mean free path, scattering inside the medium can be neglected and the transport is ballistic. Theoretical modeling of transport in the ballistic transport

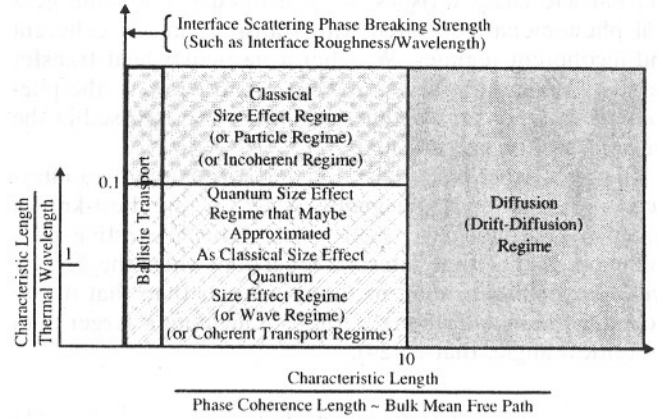

Figure 6. Different nanoscale heat transfer regimes.

regime is relatively easy. In between the ballistic and diffusive regime, both scattering at the boundary and scattering inside the medium must be considered. It is generally difficult to treat transport in this intermediate regime.

The characteristic length needs more explanation. First, the characteristic length does not have to be the structure length. As an example, in the fast heat conduction processes, a steep temperature gradient may be established over a short distance. The distance over which the temperature distribution changes significantly can be comparable to or shorter than the mean free path and in this case, size effects need to be considered. Second, a structure can have several characteristic lengths. Consider phonon heat conduction in a thin film as an example. There are two characteristic lengths. One is the film thickness and the other is the film length (or width). If the film length is much longer than the mean free path, the transport along the film plane can be described by a diffusion equation such as the Fourier law. If, at the same time, the film thickness is smaller than the mean free path, however, the thermal conductivity of the film will no longer be the same as that of the bulk constituent material of the film because lateral interfaces scatter phonons. If the lateral interface is diffuse, the transport falls into the classical size effect regime. If the lateral interface is specular, the transport falls into the quantum size regime. Thus, one can have quantized incoherent transport, quantization due to lateral interface while diffusion transport along the film plane. Electron transport in such a quantized incoherent transport regime has been studied for thermoelectric applications and it is generally agreed that the lateral quantization effect can enhance the electron energy conversion capability [30, 31]. For phonon heat conduction, however, the quantum treatment usually leads to a result that is similar to the treatment based on classical size effect treatment for a single layer thin film with specular surfaces [32] (i.e, both treatments lead to a thermal conductivity equal to that of the bulk, because the shorter thermal wavelength smears out the phonon quantization effects).

2.2. Nanoscale Heat Transfer Phenomena

With the discussion on various characteristic lengths and heat transfer regimes, we will now move on to discuss several size effects associated with three different modes of heat transfer. Because all energy carriers have both wave and particle characteristics, we will discuss first some general phenomena associated with transport in the coherent and incoherent regimes. Whether a particular heat transfer mode in a particular structure can display some of the phenomena depends on whether conditions we discussed in the previous section are satisfied.

All waves experience reflection and refraction at an interface, with the electromagnetic wave as the best-known example. For optical waves, a particularly interesting phenomenon is the total internal reflection when the refractive index of the incident medium is larger than that of the second medium and when the angle of incident is larger than the critical angle; that is [24],

$$\theta_1 \geq \theta_c = sin^{-1}\left(\frac{n_2}{n_1}\right) \tag{11}$$

where n_1 and n_2 are the refractive indices of the two media. In this case, there is an evanescent field in the second medium that does not carry a net energy into the second medium. The evanescent field decays exponentially, $e^{-x/\Delta}$, in the second medium, with a characteristic decay length

$$\Delta = \frac{\lambda_o}{2\pi n_2 \sqrt{(n_1 \sin \theta_1/n_2)^2 - 1}} \tag{12}$$

Although the example is given for an electromagnetic wave, the total reflection and the evanescent wave phenomena also exist for electrons and phonons. In addition to the evanescent wave, there can also exist surface waves that decay exponentially at both sides of the interface and propagate along the interface, such as surface plasmons which are mixtures of electron and photon waves and surface phonon–polaritons which are mixed states of photons and phonons, and surface acoustic waves [33–35]. Some of the impacts of surface waves on heat transfer processes have only recently begun to be explored [36, 37].

When there are two interfaces or the interfaces have closed topology themselves, such as the two interfaces of a thin film or the surface of a sphere/wire, the waves can experience multiple reflections inside the structure. If the phase of each reflection is preserved, the superposition of the waves creates interference/diffraction effects. The new wave functions inside the structure can also be interpreted as new energy states from quantum mechanical point of view, which can also be obtained from solving the Schrödinger equation.

If the interfaces are periodic (i.e., the structures are periodic), there can be regions (for specific wavelength and periodicity combination) in which the waves are completely cancelled and no wave exists, either in specific directions or in all the directions. An example is for electromagnetic waves traveling inside a periodic thin film structure, as shown in Figure 7. In the stop band region, the reflectivity

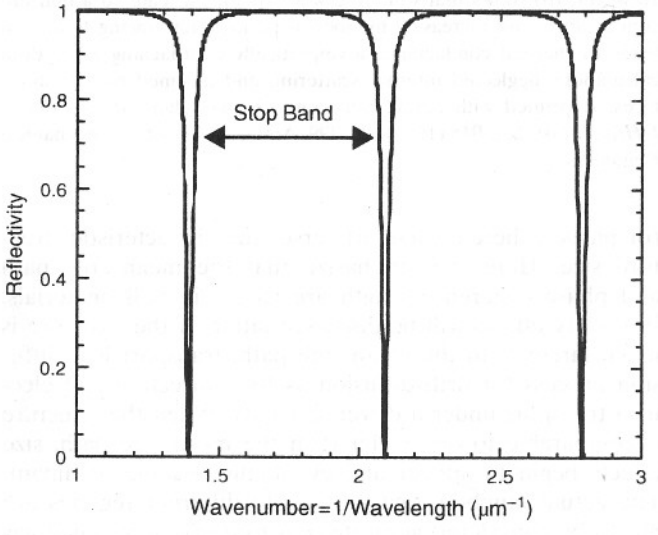

Figure 7. Calculated reflectivity of a Bragg reflector as a function of the incident photon wavelength. The refractive indices of each layer are 3 and 3.5 and the corresponding thicknesses are 417 and 352 Å for each layer, respectively.

is 100% and no waves at this frequency exist inside the film. The corresponding quantum phenomenon is the formation of electronic bandgaps that distinguish metals from semiconductors and insulators, due to the reflection of electrons in the periodic atomic potentials. Although the examples of stop bands for optical waves and that of electronic bandgap in crystalline solids have long been known, the extension of electron waves in periodic structures, such as superlattices, to form new electronic band structures [38, 39] and the extension of electromagnetic waves traveling in a three-dimensional (3D) periodic structure, to mimic what electron and phonon waves naturally do in a crystalline solids [40, 41], are relatively recent endeavors and are the precursors of the current strong drive in nanotechnology.

Wave effects offer rich possibilities because the end results depend sensitively on the phase of the waves. By changing the structures slightly, one can significantly change the phase of the waves and thus potentially engineer the transport processes. However, as discussed in the previous section, the phases are not always preserved. Phase breaking scattering events inside the solid and at the interfaces can destroy the phases and thus the wave effects. In the incoherent transport regime, the interfaces can still impact the transport because of interface scattering. These interface scattering processes generally reduce the energy flux, which can be either a problem, as for the thermal management of electronic and photonic devices [3, 4], or a blessing for other applications that demand good thermal insulation, as for thermoelectric energy conversion [6, 11].

With these general pictures, we now move on to discuss some specific heat transfer phenomena observed in nanostructures.

2.2.1. Heat Conduction

In solids, heat is conducted by electrons and phonons. In pure metals electrons dominate the conduction, while in semiconductors and insulators the dominant contribution comes from phonons. We will examine several heat conduction phenomena that are important at nanoscale, including heat conduction at a single interface, heat conduction inside thin films and nanowires, heat conduction outside nanostructures, and nonequilibrium heat conduction processes between different heat carriers.

Thermal Boundary Resistance Both electrons and phonons can be scattered at an interface. We will focus on phonons first, for which much work has been done [42]. For heat conduction perpendicular to an interface, phonon reflection implies that the energy carried by heat carriers will be reduced compared to the case when there is no interface, or equivalently, a resistance for heat flow exists at the interface. This phenomenon, called Kapitza resistance or thermal boundary resistance, has been known since the pioneering work of Kapitza [43] for liquid helium–solid interface and Little [44] for solid–solid interface, and extensive experimental and theoretical studies have been carried out in the past. At extreme low temperatures when the phonon thermal wavelength is long (Fig. 2), the interfaces are close to specular and models based on acoustic reflection and refraction for thermal boundary resistance lead to reasonably good agreement with experiment. At room temperature, however, the phonon wavelength is short and diffuse scattering can be dominant. There is no proven easy way to model the phonon reflectivity and transmissivity for such diffuse scattering processes. Two models have provided limit values for the reflectivity and transmissivity. One is the radiation model that assumes that phonons from the side with a lower maximum frequency have a unit transmissivity across the interface. By reciprocity or the principle of detailed balance, not all phonons from the side with a higher maximum phonon frequency can go over the interface. Otherwise, one side of the interface will be cooled and the other side heated, even at equilibrium. This radiation limit will provide the maximum transmissivity and thus the minimum thermal boundary resistance value. The other model, called the diffuse mismatch model, assumes that phonons are well mixed during interface scattering and there is no way to distinguish the reflected phonons from the transmitted ones on the same side (i.e., $r_{12} = t_{21}$, where r_{12} represents the phonon reflectivity for incident phonons from medium 1 into medium 2 and t_{21} is the phonon transmissivity from medium 2 into medium 1). Under this assumption, the phonon transmissivity can be expressed as [45]

$$\tau_{12} = \frac{v_2 U_2}{v_1 U_1 + v_2 U_2} \quad \text{and} \quad \tau_{21} = 1 - \tau_{12} \tag{13}$$

where U_1 and U_2 are the phonon energy density on media 1 and 2, respectively. This expression assumes a constant group velocity and is an extension of the low-temperature expression in [46]. If the phonon transmissivity is known, the thermal boundary resistance can be calculated from [46]

$$R = \frac{T_1 - T_2}{q} = \frac{2[1 - \langle \int_0^1 \tau_{12}(\mu_1)\, d\mu_1 + \int_0^1 \tau_{21}(\mu_2) d\mu_2 \rangle / 2]}{\int_0^1 [\int \tau_{12}(\mu_1) v_1 C_1(\omega)\, d\omega] \mu_1\, d\mu_1} \tag{14}$$

where $\mu (= \cos\theta)$ is the directional cosine and θ is the incident angle. This expression differs from the commonly used expression for thermal boundary resistance [44],

$$R_e = \frac{T_{e1} - T_{e2}}{q} = \frac{2}{\int_0^1 [\int \tau_{12}(\mu_1) v_1 C_1(\omega)\, d\omega] \mu_1\, d\mu_1} \tag{15}$$

because of the definition of temperature at the two sides of the interface [47, 48]. At the interface, phonons are in highly nonequilibrium states. The phonons coming toward the interface are at one set of temperatures (T_{e1} and T_{e2}), called the emitted phonon temperature (Fig. 8). These phonons, however, do not represent the local energy density because the reflected and transmitted phonons have different spectral distributions. If these phonons are assumed to approach equilibrium adiabatically, the final temperature T_1 and T_2 represents the local energy density. This latter temperature, defined as equivalent equilibrium temperature, is consistent with those local equilibrium temperature used in the Fourier law. At very low temperatures, as used in many experiments on thermal boundary resistance, one can place the sensors so that only T_{e1} and T_{e2} are measured [42]. At high temperatures, many experimental methods are based on extracting T_1 and T_2. For these cases, Eq. (14) should be used.

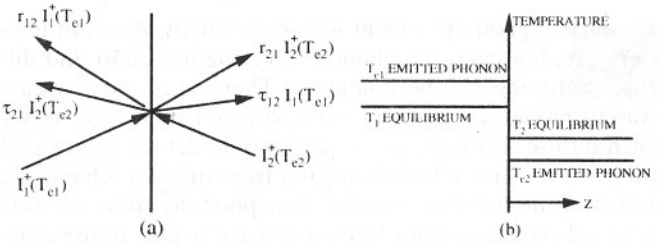

Figure 8. Illustration of phonon transport at an interface, (a) incident, reflected, and transmitted phonons, and (b) the temperature on each side of the interface. Reprinted with permission from [48], G. Chen, *Phys. Rev. B* 57, 14958 (1998). © 1998, American Physical Society.

From Eq. (14), the order of magnitude of the thermal boundary resistance is

$$R \approx \frac{2-(\tau_{12}+\tau_{21})}{C_1 v_1 \tau_{12}} \sim 10^{-9}\frac{1}{\tau_{12}} m^2K/W \qquad (16)$$

where we have used the fact that for many materials at moderate to high temperatures, $C \sim 10^6$ J/m^3 and $v \sim 10^3$ m/s. The velocity seems to be low compared to the speed of sound in many solids but is actually reasonable after considering the dispersion of the phonon spectrum. Thus, for perfect interfaces, the thermal boundary resistance is of the order of 10^{-8}–10^{-9} m^{2}K/W. This order of magnitude is consistent with molecular dynamics simulations [49] and experimental results on superlattices [50, 51].

Although this discussion is for phonons, electrons can also be reflected at an interface due to the potential mismatch at the interface. Interfacial electron transport has been studied extensively in the literature for current flow and these results can be used to predict the interface thermal boundary resistance, for example, based on the extension of the Wiedmann–Franz law from bulk to an interface [52]. If the interface is made of a metal and a dielectric, an additional energy conversion process between electrons and phonons on the metal side must be included, because eventually heat is transferred across the interface by phonons [53].

Heat Conduction in Thin Films, Superlattices, Nanowires, and Nanotubes A thin film has two interfaces. If the mean free path is longer than the film thickness, energy carriers (electrons and phonons) will be scattered more frequently at the interfaces and may experience multiple scattering. If the scattering at the interface is diffuse, as we assume for scattering due to random roughness, the thermal conductivity along the film plane will be reduced because diffuse scattering means some phonons that originally travel along the film plane direction are redirected backward. Solutions for the electrical conductivity in this classical size effect regime for a single layer of thin film, called the Fuchs–Sondheimer model, were obtained a long time ago [54–56] and are applicable to phonon heat conduction as well [3]. If the interface scattering is specular, the classical size effect model of Fuchs and Sondheimer leads to a thermal conductivity of a thin film identical to that of bulk material, because the thin film acts simply as a waveguide for the heat flow. When the film thickness is thinner than the thermal wavelength, quantum effects may be important. However, lattice dynamics calculations show that quantum effect on the energy density and group velocity leads only to a small reduction in thermal conductivity for specular interfaces [57], although there are also suggestions that the scattering mechanisms will be significantly changed, which leads to a lower thermal conductivity [58, 59]. Quite extensive studies experimentally have been carried out on the thermal conductivity of thin films. Single crystalline silicon thin films provide a model experimental system for studying the size effects, due to both the long phonon mean free path and its importance in industrial applications. In Figure 9, we show the thermal conductivity of single crystalline silicon thin films measured by several groups [60–62]. Size effects are particularly strong at low temperatures because of the increasing phonon mean free path with decreasing temperature. Polycrystalline thin films show an even larger thermal conductivity reduction, because grain boundaries greatly scatter phonons [63–70]. In the cross-plane direction, there are some measurements on the thermal conductivity of metallic and semiconducting thin films [71–73] and amorphous thin films [74–78]. Some reduction of the thermal conductivity of metallic and semiconducting thin films has been observed but the mechanisms are not well explained. For amorphous thin films, the measured thermal conductivity reduction is often explained by the inclusion of the thermal boundary resistance between the film and the substrate [74].

Superlattices are periodic thin film structures as shown in Figure 10a. Thermal properties of such structures have been studied over the last 15 years due to their importance for photonic and thermoelectric devices. Experimentally, it has been observed that superlattices have much lower thermal conductivities compared to the bulk values calculated based on the Fourier law, using the properties of their parent materials [50, 79–85]. An example of the thermal conductivity of superlattices is given in Figure 10b [83]. There are several potential explanations [11, 51]. One is the phonon spectrum change [86–91]. Figure 11a–f shows an example of the phonon spectrum of a Si/Ge-like superlattice

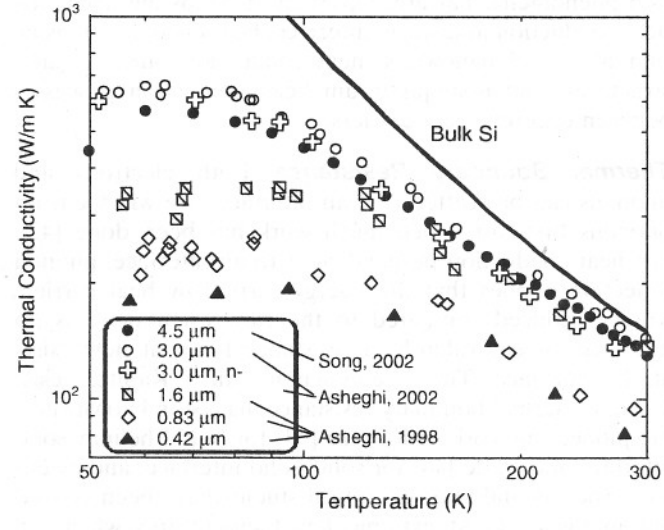

Figure 9. Thermal conductivity of single crystalline silicon thin films, showing a significant reduction as the film becomes thinner and the temperature becomes lower.

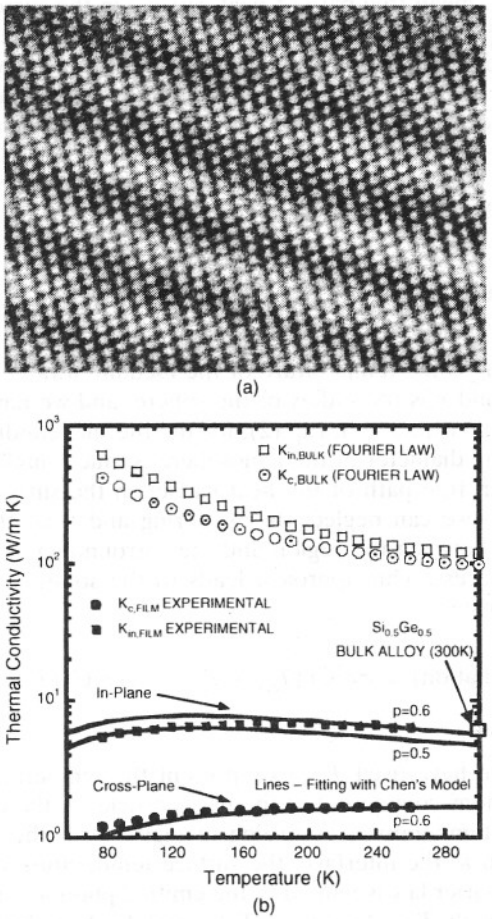

Figure 10. (a) A transmission electron micrograph of a 20 Å Si–Ge superlattices and (b) the measured thermal conductivity in both in-plane and cross-plane directions, showing a significant reduction compared to bulk values. Reprinted with permission from [83], W. L. Liu et al., *J. Nanosci. Nanotechnol.* 1, 39 (2001). © 2001, American Scientific Publishers.

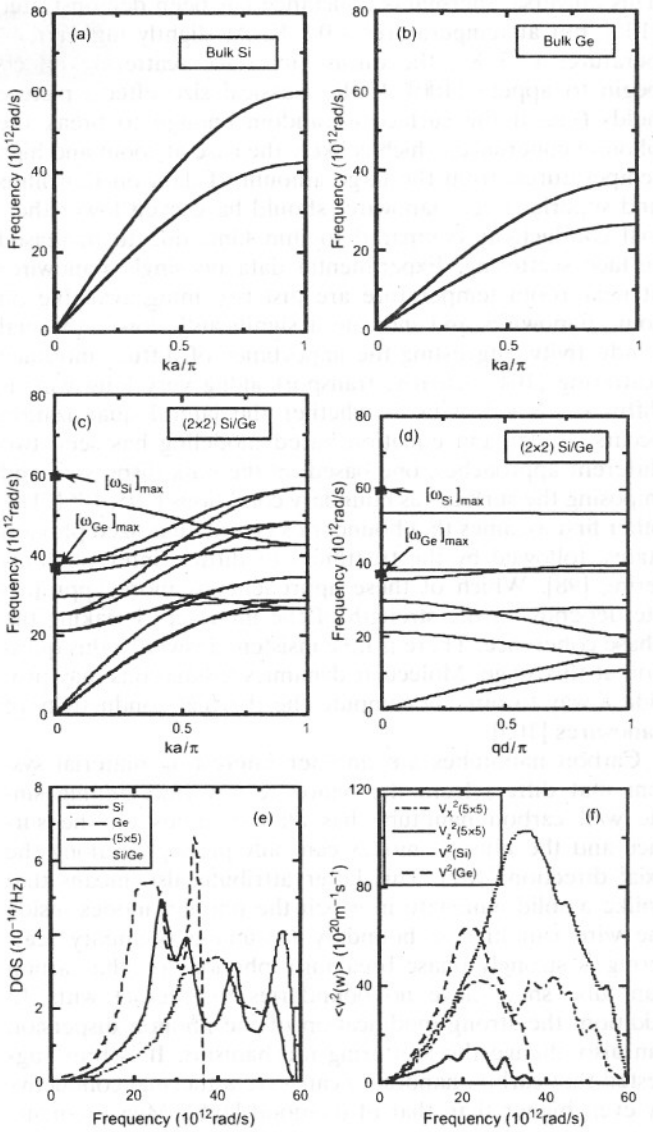

Figure 11. (a)–(d) phonon dispersion in Si, Ge, and in the in-plane (x) and cross-plane (z) direction of a Si–Ge superlattices. (e) and (f) Density of states and the group velocity. Reprinted with permission from [32], B. Yang and G. Chen, *Microscale Therm. Eng.* 5, 107 (2001). © 2001, Taylor & Francis.

calculated from lattice dynamics [32]. Compared to the phonon spectra of the bulk materials, there are several changes: (1) phonons are folded due to the new periodicity in the growth direction, (2) the acoustic phonons in the silicon layer with a frequency higher than that in the Ge layer become flat or confined due to the mismatch in the spectrum, and (3) mini bandgaps form. The impacts of these changes on the phonon density of states and group velocity are shown in Figure 10e and f. Although the change in the density of states is relatively small, there is a relatively large change in the group velocity in the cross-plane direction. This group velocity has been proposed as an explanation for the thermal conductivity reduction [89, 92]. Comparison with experimental data, however, shows that the group velocity reduction alone cannot explain the magnitude of the thermal conductivity reduction perpendicular to the film plane nor can it explain the thermal conductivity reduction along the film plane at all [32]. The reason is that the lattice dynamics model assumes phase coherence of the phonons over the whole superlattice structure and does not include the possibility of diffuse interface scattering. Models considering classical size effects lead to reasonably good agreement with experimental data [21, 48, 93]. These theoretical and experimental studies show that it is difficult to take advantage of the wave effects of phonons in phonon transport processes, primarily due to the short phonon thermal wavelength.

Thermal conductivity of nanowires is also attracting great interests [94–106]. Naturally, the interest is in for transport along the wire axis direction. Referring to the transport regime picture in Figure 6, there are several possibilities. If the surface of the wire is specular and there is no scattering inside the wire, the transport is ballistic and phonon energy states are quantized. The Landauer formalism leads to the universal phonon thermal conductance as [101, 102]

$$K = \frac{\pi^2 \kappa_B^2 T}{3h} \tag{17}$$

This universal thermal conductance has been demonstrated [101], but at temperatures <0.8 K. At slightly higher temperatures (>3 K), the diffuse interface scattering effects begin to appear [100]. If the classical size effects picture holds (i.e., if the surface is random enough to break the phonon coherence, which is likely the case at room and high temperatures, from the large amount of data on thin films and superlattices), nanowires should have even lower thermal conductivity compared to thin films due to increased surface scattering. Experimental data on single nanowires at near room temperature are just becoming available on some nanowires and indicate a significantly lower thermal conductivity, suggesting the importance of diffuse interface scattering [104]. Clearly, transport along very long wire is diffusive. A key issue is whether the lateral quantization occurs. Boltzmann equation based modeling has seen two different approaches, one based on the bulk dispersion and imposing the surfaces as boundary conditions [105, 106]. The other first assumes that boundaries create quantized phonon states, followed by the treatment of diffuse interface scattering [98]. Which of these approaches is more appropriate depends on the strength of the interfaces breaking the phase coherence. There is no consistent answer to this question at this stage. Molecular dynamics simulations may provide a way to directly compute the thermal conductivity of nanowires [105]

Carbon nanotubes are another interesting material system that differs from the nanowires. A freestanding single wall carbon nanotube has all the atoms on the surface and the phonon modes can only propagate along the axial direction [107]. This latter attribute also means that unlike a solid nanowire in which the phonon modes inside the wire can hit the boundary (assuming boundary scattering is strongly phase breaking), phonons on the carbon nanotube sheet have no boundaries to interact with. In addition, the strong modification of the phonon dispersion can also change the scattering mechanisms. It is thus suggested that carbon nanotubes can have a thermal conductivity even higher than that of diamond [108]. Measurements and simulation data so far vary widely. Molecular dynamics simulations carried out by various group also have widely varying thermal conductivity values [109–113]. Similar is the case of experimental studies. Measurements on an isolated multiwall carbon nanotubes lead to high thermal conductivity values [99] but measurements on tangled and aligned carbon nanotubes have values orders of magnitude smaller [114–116]. At this stage, the reasons for such large discrepancies are unclear. It is quite possible that although a freestanding nanotube has high thermal conductivities, a nanotube embedded in a host sees increasing interface scattering which reduces its thermal conductivity values. Continued study on this issue is important for the potential applications of carbon nanotubes.

Rarefied Phonon Heat Conduction External to Nanostructures Although the thermal conduction reduction in thin films and nanowires is a well-known phenomenon, the size effects outside for heat conduction external to nanostructures have not received much attention. Heat generated inside nanoscale regions or nanostructures eventually will be conducted to the surrounding. When the heat generation region or the size of the nanostructure is smaller than the mean free path of heat carriers in the surrounding medium, the temperature rise of the nanostructure can be much higher than that predicted by the Fourier law [117]. To see why this occurs, we consider the heat conduction surrounding a heat generating spherical region embedded inside a semi-infinite medium. The Fourier law leads to the relation between heat transfer rate, Q, and the temperature rise at the surface of the sphere, T_s,

$$Q(\text{Fourier}) = 4k\pi r(T_s - T_\infty) = \frac{4\pi}{3} rCv\Lambda(T_s - T_\infty) \quad (18)$$

where T_∞ is the temperature of the medium away from the sphere and r is the radius of the sphere, and we have used the kinetic expression, Eq. (2), for the thermal conductivity. When the diameter of the nanosphere is much smaller than the mean free path of the heat carrier in the surrounding, however, we can neglect the scattering and treat the heat transfer between the region and the surrounding as a radiation process. This approach leads to the solution for the heat transfer,

$$Q(\text{radiation}) = \pi r^2 Cv(T_{s,e} - T_\infty) \approx 2\pi r^2 Cv(T_s - T_\infty) \quad (19)$$

where we have used $T_{s,e}$ to represent the temperatures of the phonons coming out of the nanoparticle, or the emitted phonon temperatures according to Figure 8. If there is no reflection at the interface, the surface temperature as used in the Fourier law is related to the emitted phonon temperature through, $T_s = 0.5 \cdot (T_{s,e} + T_\infty)$, which leads to the second equality of Eq. (19). Comparing Eq. (19) with Eq. (18), we can see that

$$\frac{Q(\text{Fourier})}{Q(\text{Radiation})} = \frac{2\Lambda}{3r} \quad (20)$$

Thus, in the limit where the mean free path is much larger than the sphere radius, the Fourier law overpredicts the heat transfer rate. This is because the Fourier law is only applicable when there is not a large temperature gradient within one mean free path. For the previous example, the application of the Fourier law to a region much smaller than the mean free path (surrounding the sphere where temperature varies significantly) inherently implies that there is strong scattering in this region, which is only true when the mean free path is much smaller than the region, while in reality, the mean free path corresponding to the bulk thermal conductivity is much larger.

Several theoretical studies have investigated the rarefied heat conduction cases, including transient heat conduction for planar geometries [118, 119], steady state in a spherical geometry [117], and in more complicated device structures [120, 121]. Experimentally, the rarefied heat conduction effect is proposed to explain the fabrication of nanostructures by scanning tunneling microscopy [122]. A recent experiment by Sverdrup et al. [123] provides evidence of the effect. More experimental studies are needed to demonstrate this phonon rarefaction effect beyond doubt.

Nonequilibrium between Carriers In dealing with nanoscale heat transfer, it is important to identify where and how heat is generated and how heat is exchanged between different groups of heat carriers. For example, in the fast laser heating of metals, electrons usually first absorb the photon energy and relax the energy to phonons [124–126]. Depending on the electron–phonon heat exchange rate and the rate of heat input, the electrons can be heated to a much higher temperature than the phonons. Similarly, electrons under a high electric field can be heated to a temperature much higher than that of the lattice [23]. Such "hot electron" effects have been extensively studied for electronic devices. Because electrons and phonons travel at a different rate, with the electrons much faster, hot electrons can significant change the heat source distribution. For example, most heat in a MOSFET (metal-oxide-semiconductor field-effect transistor, the most important device for very-large-scale integrated circuits such as microprocessors and semiconductor memories) is generated in the drain side where hot electrons dump their energy [127]. The release of heat from electrons to phonons can also significantly affect the lattice temperature rise. For example, electrons interact more readily with optical phonons, particularly polar optical phonons as in GaAs [128, 129]. The optical phonons, however, do not carry heat as efficiently as acoustic phonons. Consequently, depending on the energy exchange rate between optical phonons and acoustic phonons, hot optical phonons can be generated. Due to the large dispersion of acoustic phonons, it is also possible that acoustic phonons are significantly out of equilibrium with each other. There are also possibilities to create cold electrons relative to the lattice temperature, which can be utilized for thermoelectric refrigeration [130]. Studies on the impacts of nonequilibrium between energy carriers and within the same type of carriers on heat transfer processes are relatively scarce.

2.2.2. Thermal Radiation

Photons can have a long mean free path as evidenced by the solar radiation traveling to the earth and can also have a very short mean free path as the rapid decay of electromagnetic waves inside a metal. The studies of radiation heat transfer thus have traditionally spanned the ballistic to the diffusive regime [25]. Because of its short thermal wavelength, most research on thermal radiation falls into the classical size effect regime (i.e., ignoring the phase of electromagnetic waves). Compared to phonons and electrons, however, the thermal wavelength of the photons is actually very long, as clearly shown in Figure 2, and it is much easier to observe wave effects for thermal radiation than in heat conduction. Thus, the most interesting aspect of radiation heat transfer in nanostructures comes from the wave aspects of thermal radiation.

Interference effects on radiative properties of thin films have been studied [131–137]. Because of the interference effects, radiation properties, such as emissivity of thin films, can be thickness dependent. Such thickness dependence may be important for emissivity control and for the temperature control of surfaces. In nonplanar geometries, diffraction effects can also significantly change the radiative properties [138]. While these effects are relatively well known, more exciting recent advancements occur in the photonic-crystal structures that are an extension of the periodic thin film structures as Bragg reflectors into 2D or 3D structures [139–142]. Similar to the electron band structure formation in periodic atomic potential, photon energy states in such periodic structures form bands and for appropriate geometries, absolute bandgap can form such that no radiation can exist in any direction. This opens the potential of emissivity control both spectrally and directionally.

Radiation tunneling is another interesting phenomenon that has been studied for its heat transfer implications [13, 14, 143–146]. From Eq. (12), we can see that an evanescent wave extends over a distance of the order of a wavelength under the total reflection condition. This evanescent wave can become propagating if a third medium is brought close to the interface between the first and second media. When this happens, total reflection no longer happens and electromagnetic waves originally confined within the first medium can deliver energy into the third medium. This phenomenon is called tunneling. Tunneling can lead to, for example, increased heat transfer between the two parallel plates, even above the radiation heat transfer between two blackbodies [14, 144].

A very interesting recent development is the exploration of surface waves such as surface plasmons and surface phonon–polaritons [36, 37, 147–150]. Surface waves exist only at specific frequencies. The surface modes decay exponentially away from the surface and are normally not useful. However, just as in the case of tunneling, the surface mode can tunnel into a third medium if it is brought into close proximity to the first interface. An example is shown in Figure 12, which shows the increased radiation heat transfer at the surface phonon–polariton frequency of boron nitride [151]. These surface modes can also be coupled by grating structures into propagating waves in free space [148]. Because the surface waves have a relatively long mean free path and because the surface modes exist only in a narrow wavelength range, the thermal emission from such surface modes can be coherent and nearly monochromatic.

These discussions focus on the photon transport. Another effect of nanostructures is to change the optical constants. For example, the energy spectrum change of electrons and phonons due to quantum size effects will create subsequent change on the optical constants. Another example is the anomalous skin effect that occurs when the electromagnetic field varies strongly over the mean free path of electrons, similar to the nonlocal phonon heat conduction effects [19, 152]. The impacts of these changes on radiative heat transfer have not been explored, except the anomalous skin effects.

2.2.3. Convection

Convection is a process concerned with heat exchange between a solid surface and a fluid. The energy transfer in convection is due to both molecular diffusion and bulk motion of the fluid in the presence of a temperature difference. As in conductive and radiative heat transfer, convection may also experience size effects. For example, the mean free path of gas molecules becomes comparable with

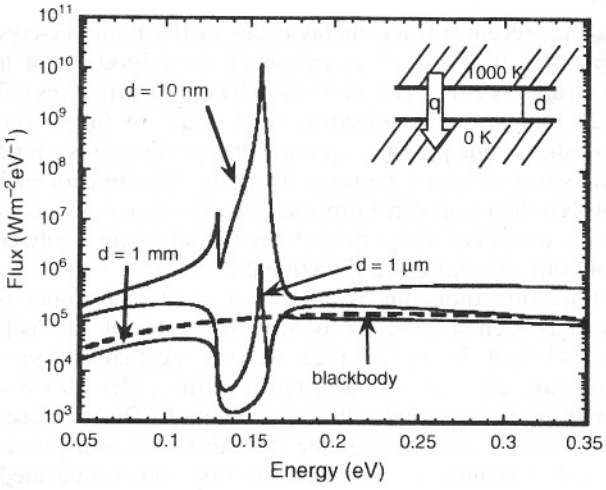

Figure 12. Spectral radiative energy transport between two half-planes of cubic boron nitride separated by a layer of vacuum of thickness d. Adapted with permission from [151], A. Narayamaswany and G. Chen, "Surface Modes for Near Field Thermophotovoltaics," unpublished.

the characteristic length of a nanostructure even at atmospheric pressures, as shown in Figure 1. This situation is similar to heat transfer in gases of low pressures and can be described by the rarefied gas theory [153]. Characteristic to this regime is the thermal creep or thermal transpiration where gas molecules creep from the cold side to the hot side along a channel with a diameter comparable to the mean free path [153]. In the case of small particles subjected to a temperature gradient this phenomenon may induce particle levitation due to thermophoresis [154]. On the other hand, liquid molecules are closely packed and have short-range interactions. Typically the continuum theory can be used to describe liquids layers as thin as 5–10 molecular diameters [155], although close to a solid surface other phenomena such as wetting, adsorption, electrokinetics, and dielectrophoresis may have to be considered [156, 157].

One way to control thermal properties of liquids is the addition of small particles to the liquid. Studies of effective thermal conductivity of solid suspensions date back to Maxwell's work on effective media theory [158]. However, recently it has been observed that the addition of nanometer size particles dramatically changes transport properties and enhances heat transfer performance of the liquids [159]. The mechanisms for enhanced heat transfer in nanofluids are not well understood [160]. Further theoretical and experimental studies are required to understand them.

3. APPLICATIONS

Energy generation and transport is a fundamental process essential to many engineering applications. Nanoscale heat transfer phenomena discussed previously have impacts on a wide range of contemporary technologies from microelectronics to bioengineering. The unusual heat transfer physics in nanostructures also opens new ways to tailor materials' properties, which in turn may lead us to innovative applications. We illustrate here with a few examples in information technologies, energy technologies, material processing, and biotechnology.

3.1. Information Technologies

Nanoscale heat transfer phenomena discussed previously have important implications for microelectronics, optoelectronics, and data storage technologies. The thermal management of microelectronics has already become a challenging issue. Nanoscale heat transfer effects may further complicate the problem [3]. Figure 1 shows that the phonon mean free path in silicon at room temperature is ~250 nm, longer than the channel length of a MOSFET device. In addition, heat is mostly generated in the drain side over a lateral dimension ~10 nm. The rarefied phonon heat conduction effect discussed before means that the Fourier law underpredicts the device temperature rise. In addition, the nonequilibrum between optical and acoustic phonons can further increase the local temperature rise. As the gate length continues to decrease, it is also predicted that the operating voltage cannot correspondingly be reduced for maintaining a low leakage current [161]. Cryogenic operation of electronic devices is being seriously considered by the microelectronics industry to improve performance. The phonon rarefaction effect will be more significant at lower operation temperatures (i.e., the deviations from the predictions of the Fourier law will become larger), because of the increasing phonon mean free path in bulk materials with decreasing temperature. How this effect will impact the scaling of microelectronic devices has not been carefully examined.

Another key component of current technological applications is semiconductor diode lasers which are usually made of multilayer thin films. Two major types of semiconductor diode lasers, edge–emitting lasers and vertical-cavity surface emitting lasers (VCSELs), are currently commercialized and used in a wide range of applications including laser printers and high density optical disks, playing a central role in today's optical communications. The excessive temperature rise in VCSELs, partly due to the high electrical resistance created by the heterointerfaces and partly due to the low thermal conductivity of the multilayer structures, had been the road block for their commercialization until a few years ago [4]. Studies on the thermal conductivity of superlattices were partly motivated by this issue. Although this problem has partly been solved for some low power applications, heating is still the most important factor limiting the power output and is more severe for near infrared lasers due to the large nonradiative recombination that is eventually converted into heat [162–165]. Edge emitting devices have less of a heating problem than VCSELs but facet damage is often associated with heating [166]. The high power outputs required to achieve reliable optical performance coupled with the low thermal conductivity of multilayer thin film structure often result in a short device life [4, 167]. The reduced thermal conductivity calls for careful design of the devices to minimize the number of interfaces and to allow efficient heat removal from the gain region.

While heating in integrated circuit and in semiconductor lasers is undesirable and needs to be "managed," it is actually used extensively as a means for writing data onto storage medium such as CDs and magnetic hard drives. For

magnetic hard drives, one of the major factors that determine data storage density is the separation between the slider and the magnetic disk known as the flying height. In present-day hard drives the flying height is around 50 nm while the disk rotates at ~10, 000 rotations per minute. The airflow between the slider and the disk is crucial in maintaining the height of the disk and is very different from the prediction of continuum fluid mechanics at this small spacing [168]. Another factor to be taken into account is the thermal creep [168], and this effect has also been proposed for novel levitation-based recording systems [169]. Equally important to the storage density is the size of the magnetic domain. It is difficult to increase the storage capacity of current magnetic disks beyond a density of 40 Gb/in^2 [170] because of the superparamagnetic effect that affects magnetic domain stability. New magnetic materials with larger magnetic anisotropy are being developed [171] and heating has been proposed as a means to assist the writing processes [8, 172, 173]. Meanwhile, alternative technologies are being developed. Some rely again on heating, such as thermomechanical data storage, where data bits are written on polymer substrates by heated atomic force microscope (AFM) tips. A storage density as high as 400 Gb/in^2 has been demonstrated [8]. The writing process as well as the data reading requires highly localized spatial and temporal heat deposition. Many rewritable CDs are based on the phase change caused by laser heating [174–176]. For such applications, it is desirable to limit the heating within a small domain. Nanoscale heat transfer effects including reduced thermal conductivity of thin films and nonlocal heat conduction surrounding nanoscale heating spots can be utilized to confine heat for writing smaller spots.

These examples emphasize the small length scales involved in nanodevices and nanomaterials. A short time scale is also becoming increasingly important. Similar questions can be raised for transport at short time scales as for the small length scales. Lasers can deliver a pulse as short as a few femtoseconds (1 fs = 10^{-15} s). Energy transduction mechanisms at such short time scales can differ significantly from that at macroscale [126]. Microelectronic devices are pushing to the tens of gigahertz clock frequency with a much shorter transient time. The device temperature rise in such short time scales can be very different from predictions of the Fourier law.

3.2. Energy Conversion

Energy conversion is a field that may greatly benefit from nanoscale energy transport phenomena. An example is thermoelectric cooling and power generation based on the Peltier effect and the Seebeck effect, respectively [177]. The efficiency of a thermoelectric device is determined by the thermoelectric figure-of-merit of the material $ZT = \sigma S^2 T/k$, where S is the Seebeck coefficient, σ is electrical conductivity, k is the thermal conductivity, and T is the absolute temperature. Currently, the best commercially available thermoelectric materials based on Bi_2Te_3 and its alloys has a ZT of ~1. Thermoelectric devices based on this material cannot compete in performance with other well-established technologies for energy conversion. Several approaches have been explored to increase the thermoelectric figure-of-merit [5, 178]. Among those, low-dimensional thermoelectric materials structures such as quantum wells, superlattices, and nanowires have been extensively investigated [179-183]. Quantum size effects on electrons in nanostructures can be utilized to improve the electron energy conversion capability [30], while the reduced thermal conductivity of nanostructures due to increased scattering of heat carriers from interfaces can be exploited in reducing the denominator of ZT. In the past two years, different low-dimensional thermoelectric materials that show improved cooling capacity as compared to bulk materials have been reported [185, 186]. This suggests that phonon engineering is a primary tool in developing better thermoelectric materials.

The wave effects on radiation heat transfer can be utilized for thermophotovoltaic energy conversion in different ways. Photonic crystals can have the spectral emissivity tuned to match the bandgap of semiconductor photovoltaic cells [187]. Tunneling effects are being explored to increase the energy density delivered from the heat source to the photovoltaic cells [13, 188]. Surface waves, such as surface plasmons and surface phonons, can be utilized for nearly monochromatic thermal radiation, which increases the efficiency of thermophotovoltaic energy conversion [36, 151, 189] as well as the energy density if small gaps are employed to take advantage of the high energy density of surface waves.

3.3. Nanomaterial Synthesis and Nanofabrication

Nanomaterial synthesis and nanostructure fabrication are two areas where thermal transport is often important but has received less attention. Size-dependent melting point depression of nanoscrystals may be used to develop techniques for fabrication of cheap electronics [190]. A different example is related to multilayer structure masks currently used in extreme ultraviolet lithography and X-ray lithography [191]. The heat generation in these structures and its impact on the structural fabrication accuracy has yet to be investigated. Ultrafast laser nanomachining [192] and nanoimprint lithography [193], both based on short time interaction of a laser pulse with sample surface, also call for better understanding of flow and heat transfer at nanoscale and short time scale. The synthesis of nanoscale materials is a wide-open field and many nanomaterial and nanostructure synthesis methods being developed raise intriguing nanoscale heat transfer questions. For example, nanowires and carbon nanotubes have been made with different methods such as chemical or physical vapor deposition, filling of templates through liquid phase, vapor deposition, and electrodeposition [194–198]. Understanding the transport processes during nanomaterial formation will allow better control of the final material quality. Scanning probe based fabrication methods also often involve nanoscale heat transfer issues that are not well understood. For example by focusing a laser beam onto an AFM or scanning tunneling microscope tip, structures with dimensions down to 10 nm can be fabricated [199, 200]. In a different experiment an infrared laser is focused on an AFM tip

in contact with a PMMA substrate to produce pits of several hundreds Å in size [201]. Understanding the interaction between electromagnetic radiation and nanostructures and its coupling, the heat conduction, is obviously very relevant for improving these fabrication methods.

3.4. Biotechnology

Nanoscale heat transfer is also making in-roads in biotechnology. Inductively heating gold nanoparticles attached to DNA strands has been found to be a promising method to control DNA hybridization [202]. The heat transfer mechanism between the nanoparticle and DNA strand has yet to be elucidated.

4. EXPERIMENTAL TOOLS

There are two key experimental directions in studying nanoscale heat transfer phenomena. One is the thermophysical property measurements of nanostructures such as thin films and nanowires. The other is the temperature measurements, particularly temperature mapping surrounding nanoscale devices. In this section, we briefly describe some of the techniques used for thermophysical properties characterization and temperature measurement of nanometer size samples. Additional details can be found in reviews on similar topics available in the literature [11, 64, 203–205].

4.1. Thermophysical Properties Characterization

Measuring thermophysical properties is always a challenging task, even at macroscale. The thermophysical property characterization of nanostructures and microstructures is even more challenging. The measurements of the thermal conductivity, for example, normally require the determination of heat flux and temperature drop between two points of the sample, which becomes much more difficult in nanostructures than in macrostructures. Taking thin films as an example, the measurement of thermal conductivity perpendicular to the film plane (cross-plane direction) requires the determination of the temperature drop over the film thickness that ranges from nanometers to micrometers. Because thin films are often deposited on substrates, it is difficult even to create a reasonable temperature drop across the film without creating a large temperature rise in the substrate, not to mention determining the temperature drop across the film. The thermal conductivity measurement parallel to the film plane (in-plane direction) may look easier because temperature sensors can be placed along different locations in the film surface. However, the substrate makes difficult the determination of actual heat flow in the film. To overcome these difficulties, different strategies have been developed for measuring thin film thermal properties in different directions. In the cross-plane direction, the general strategies are (1) creating a large heat flux across the film while minimizing the heat flux in the substrate and (2) measuring the surface temperature rather the temperature drop. These can be realized by, for example, using microfabricated heaters directly deposited on the film. By using a small heater width, the heat flux is large when going through the film but the heat spreading inside the substrate significantly reduces the temperature drop in the substrate. Another example is to use transient or modulated heating that can limit the heat affected region close to the film. In the in-plane direction, one often used strategy is to remove the substrate such that the heat flux through the film can be uniquely determined.

In the following, we will first discuss thin film thermophysical property measurements and divide our discussion based on different heating and temperature sensing methods: the electrical heating and sensing based on microheaters and sensors, the optical heating and sensing methods, and the combined electrical/optical methods. After these discussions, we will review several methods used for nanowire property measurements.

4.1.1. Electrical Heating and Sensing Based on Microheaters and Microsensors

Microheaters and sensors can be fabricated onto the samples using microlithography techniques developed in the semiconductor industry. In some methods, the heaters are also used directly as the temperature sensor while in other techniques, separate heaters and temperature sensors are used. The advantages of the electrical heating and sensing methods, compared to optical heating and sensing, are that the amount of heat input into the sample can be precisely controlled and the temperature rise can be accurately determined. By using microheaters and microsensors, high heat flux can be created and temperature rise can be pinpointed at micrometer scales, depending on the sensor dimension. We will further divide our discussion for measurements in the cross-plane and in-plane directions.

Cross-Plane Thermal Conductivity Measurement of Thin Films One major method for measuring the cross-plane thermal conductivity of thin films is the 3ω method, initially developed for measuring the thermal conductivity of bulk materials and later extended to thin films [74, 206]. Thermal conductivity of thin films down to 20 nm in thickness has been measured using this technique [74, 206, 207]. The method has also been adapted for simultaneous measurement of the in-plane and cross-plane thermal conductivity of anisotropic thin films [83] and freestanding membranes [208]. In the 3ω method a thin metallic wire is deposited onto the sample surface to act as both a heater and a temperature sensor. An ac current with angular modulation frequency (ω) passing through the wire causes Joule heating and ac temperature oscillations of the wire with a frequency of 2ω. Due to the temperature dependence of the electrical conductivity, the resistance also has a 2ω component proportional to the ac temperature rise. The voltage drop along the wire thus contains a third harmonic (3ω) component that depends on the ac temperature rise of the heater. Since the heater measures only the temperature rise on the front surface (T_f), the temperature rise at the interface between the film and the substrate (T_s) must be determined. This can be done by two approaches. One method, often referred to as the slope method, is to calculate the temperature rise at the film–substrate interface based on the thermal conductivity of the substrate. The latter can be determined

from the frequency dependence of the measured front surface temperature [206] because the temperature drop across the film itself is frequency independent when the film is thin. Figure 13a shows an example of measured temperature rise at the front surface and inferred substrate temperature.

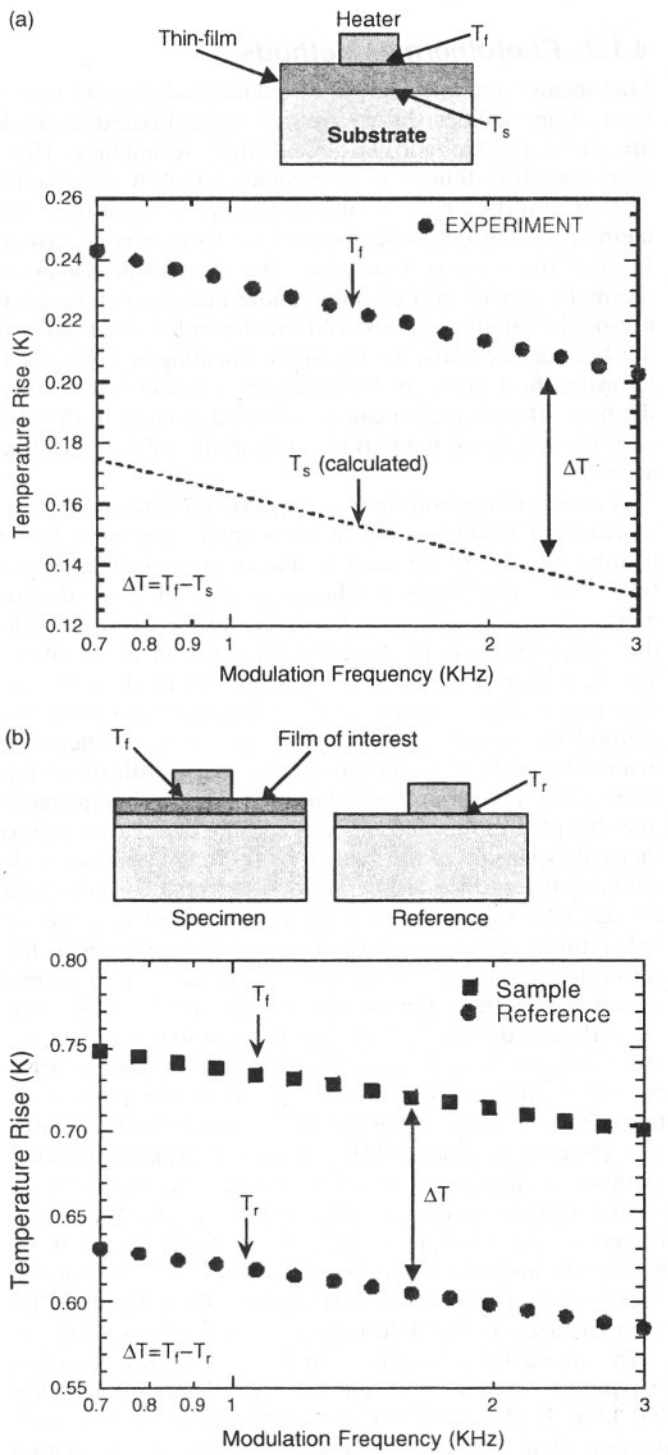

Figure 13. (a) Experimental temperature rise (T_f) and calculated substrate temperature (T_s) in the slope method. (b) Experimental temperature rise for the specimen (T_f) and reference sample (T_r) in the differential method.

Detailed modeling, however, shows that the determination of the substrate thermal conductivity based on the front side temperature measurement is prone to error when the film is relatively thick. A different way to estimate the temperature drop across the thin film is to measure it experimentally by a differential technique [209], which measures the difference of the front surface temperature rise between the actual sample and a reference sample that does not have the film. An example of the temperature rise measured by the heater onto the specimen (T_f) and reference sample (T_r) is shown in Figure 13b. Usually, the heater width is chosen to be much wider than the film thickness such that heat conduction across the film can be treated as one-dimensional (i.e., in the cross-plane direction only). Although simplified one-dimensional steady-state models are often used in extracting the cross-plane thermal conductivity of the thin film, it is important to carry out more detailed modeling when the contrast in properties between the film and the substrate becomes small. By choosing heaters of different width, for example, through the use of two heaters, one with a width much larger than the film thickness such that it is most sensitive to the cross-plane thermal conductivity, and the other with a width comparable to the thickness such that lateral spreading effect is important, both in-plane and cross-plane thermal conductivity of the thin films can be determined [83, 209].

The modulation technique as used in the 3ω method has several advantages. One is that the ac temperature field can be controlled by the modulation frequency. With reasonably high modulation frequency, the ac temperature field is confined to the region close to the heater such that the substrate can be treated as semi-infinite. This avoids the influence of the boundary condition at the substrate side. Another advantage of the modulation technique is that the ac signal is less sensitive to the radiation heat loss compared to dc measurement methods. The ac modulation also leads to the possibility of determining the substrate properties in addition to the film properties.

In addition to the 3ω method, a multisensor steady-state method was developed to measure the thermal conductivity of SiO_2 thin films deposited on silicon [210, 211]. This method relies on the temperature measurements by adjacent sensors to back up the temperature underneath the heater. Because the measurement is done at the steady state, the boundary condition at the back side of the substrate is important for determining the temperature underneath the heater.

In-Plane Thermal Conductivity Measurements Several in-plane thermal conductivity measurements have been developed by making freestanding thin film structures [65, 212, 213]. One of the configurations is to fabricate heater and temperature sensors on a large membrane as schematically shown in Figure 14a. Heat generated from the heater spread from the membrane to the frame. The other configuration shown in Figure 14b is to further shape the membrane into a narrow line and to pass current directly through the line, if the membrane is conducting or semiconducting. In this case, heat spread out along the line axis direction and the average temperature of the line is measured and correlated to the thermal conductivity.

Depending on the thermal conductivity of the film to be measured, there are several considerations one should pay

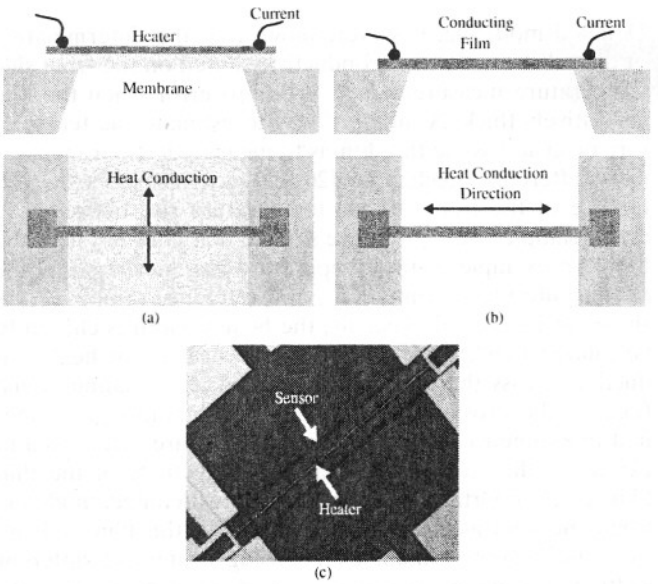

Figure 14. In-plane thermal conductivity measurement based on (a) membrane and (b) bridge structures. A fabricated membrane with the heater and the temperature sensor is shown in (c).

attention to. If the membrane method is applied to measure the thermal conductivity of a low thermal conductivity film, the structure should be designed such that heat conduction is one-dimensional, otherwise two-dimensional simulation must be carried out to back up the thermal conductivity of the film. For low thermal conductivity films, heat leakage through the heater itself may be a significant component of the total heat transfer, and thermal radiation and convection loss can further increase the uncertainties in determining the thermal conductivity. Sometimes, two different membranes are used to determine the thermal conductivity, by assuming that the effective heat transfer coefficients for both geometries are the same [212, 214]. This assumption is dangerous if the experiment is done in air because natural heat transfer coefficient scales with the heated area. Ac- or transient-based heating and measurements can reduce the effects of heat loss through the metal heater and by thermal radiation [215]. If the measured membrane has a relatively high thermal conductivity, the spreading thermal resistance in the substrate supporting the membrane can be important. Multiple temperature sensors sometimes are fabricated along the membrane to eliminate this uncertainty but the additional loss along these temperature sensors should be considered [216]. A better location is to place the temperature sensor on the substrate at the place where the membrane meets the substrate, as shown in Figure 14c.

The bridge method constrains the heat flow to one dimension [65, 212, 217]. In this sense, it avoids the potential complication of the two-dimensional heat conduction effects in the membrane. However, the thermal conductivity depends on temperature profile along the bridge, which further depends on the radiation and convection heat losses and on the thermal resistance at the two ends of the bridge. In addition, the method is only applicable if a current can pass through the film (or another conducting film with known properties is deposited onto the film).

In addition to removing the substrate, we also mention the 3ω method to measure the in-plane thermal conductivity by exploring the heat spreading effect with small heaters [83, 209, 218]. When a high thermal conductivity film, such as silicon, is separated from the substrate by a low thermal conductivity layer, such as SiO_2 [22], surface temperature can also be sensitive to the in-plane thermal conductivity [76].

4.1.2. Photothermal Methods

Microheater and microsensor based methods require microfabrication facilities. In comparison, optical based methods are more flexible and are noncontact techniques. However, since it is difficult to determine accurately the amount of heat absorbed by the sample, the optical heating based methods usually do not lead directly to thermal conductivity. Instead, these methods measure the thermal diffusivity or thermal effusivity of the sample under investigation by monitoring the sample response to time dependent heat input at the boundaries. Pulse or modulated heating is often used. By using short pulses or high frequency modulated heating, the heat affected region can be confined to close to the film such that excessive temperature rise in the substrate can be avoided.

A variety of methods have been developed based on modulated laser beam heating of the sample. The modulation heating is favored because it allows phase-locked detection of the temperature-induced signals. In these experiments, a modulated laser beam (pump) is focused onto the sample surface, producing a local rise in temperature. The detection of temperature increase can be done by various means. For example, in the photothermal reflectance method, the sample reflectivity is monitored by another laser beam (the probe) focused on same location with the pump beam [219]. The photothermal displacement technique monitors the physical displacement of another laser beam due to thermal expansion of the sample [220]. In the photoacoustic methods the surface temperature is detected by measuring the acoustic signals coupled to the piezoelectric detectors either through the air on the front surface or through the substrate to the back surface [221]. In the photothermal radiometry method, the blackbody radiation from the sample surface is detected [222]. Another way to detect temperature increase is to measure the deflection of a laser beam parallel to the sample surface, caused by the gradient of the refractive index of the gas layer adjacent to the heated spot (Mirage method) [223]. The photothermal reflectance method can also be employed to visualize the thermal wave on the surface of the sample, by moving one beam with respect to the other [224, 225]. Typically the pump beam is scanned and the probe beam remains fixed in order to avoid surface roughness effects on the reflected beam. This technique may reveal defects or grain boundaries [225].

The modulation frequency in the techniques described is typically limited to a few megahertz and often below 100 kHz. Under such modulation frequency, the ac temperature field penetrates into the substrate. Interpretation of the photothermal signals thus involves the substrate thermophycial properties. Although the latter may also be determined from the measured signal, the inclusion of the substrate thermophysical properties as unknowns also can

cause more uncertainty in the film thermophysical property determination. A method to avoid the effects of the substrate is the transient photothermal technique [226], often called pump-and-probe technique, where the transient heating pulse ranges from nanosecond to femtosecond. The main advantage of using pulse lasers is that, for a particular pulse regime, the penetration depth of the thermal wave may be small compared with film thickness. Therefore heat diffusion at nanometer length scale can be measured directly. When picosecond or femtosecond pulse lasers are used, it is not possible to detect such fast changes in temperature with typical measurement instrumentation. In this case, the temporal response is measured by delaying the probe pulse with respect to the repetitive pump pulse and measuring its reflectivity for various delay times. Other experimental setups of this technique use nanosecond lasers [227]. In this case the temperature decay is still measurable by fast radiation detectors.

Photothermal methods have been used for measuring thermophysical properties of a wide range of materials such as metallic, semiconductor, or dielectric films [219], and superlattices [80] as well as for studying grain boundaries in semiconductors [228], interface thermal contact resistance [227, 229], and thermal properties colloid metal particles [230].

4.1.3. Mixed Optical/Electrical Heating and Detection Methods

There are also several methods that employ optical heating and sensor detection, or electrical heating and optical detection. Ac calorimetry is an example where optical heating is combined with thermocouple detection, if the response time requirement is not high, as in the measurement of low thermal diffusivity samples [204]. Thermal diffusivity of the sample is determined by measuring the temperature rise at different distances from the heated spot using fine thermocouples [204] or resistive thermometers [231]. Under appropriate conditions, the thermal diffusivity along the film plane can be calculated from phase or amplitude data. Cross-plane thermal diffusivity measurement is also possible by detecting the temperature rise at the back side of the sample with a thin resistive thermometer [231]. A different way to detect the thermal response of optically heated samples is to use a fast thermoelectric effect. In photothermoelectric technique, the specimens are heated on one side by laser radiation or white light collected from a high power lamp [232, 233]. The temperature is measured on the other side by a fast responding thermocouple, which consists of the contact point between a sharp wire and the electrically conductive sample surface. The technique may be employed in thermal diffusivity measurement of freestanding films or thin films on substrates transparent to the heating beam. In addition the light spot can be scanned around the detection point to image the thermal wave on sample surface. In addition to optical heating, electrical heating is also combined with optical detection to determine the thermal diffusivity of thin films. For example, electrical heating is combined with thermal-reflectance change or thermal emission to determine the thermal diffusivity of thin film [227, 234].

4.1.4. Nanowires and Carbon Nanotubes

While the experimental methods for thermal characterization of two-dimensional structures are relatively mature, only a few attempts have been made toward thermal property characterization of one-dimensional structures. Earlier experiments on thermal transport in one-dimensional structures have been carried out by Potts and co-workers [95–97]. The motivation of the work was to observe phonon quantization in nanowires made of GaAs single crystal that is known to have a large phonon mean free path. Freestanding arrays of highly doped GaAs are resistively heated, as in the bridge method for thin film thermal conductivity measurement. Their experiment, done at cryogenic temperatures, shows that electrons and phonons are at nonequilibrium and the measured thermal conductance is due to the electron conduction. Related to the nonequilibrium interactions are the experiments of Seyler and Wybourne on the electrical conductivity of metallic nanowires on silicon substrates [94]. They observed local peaks in the electrical resistance as the dc field applied across the wires was increased. The results were explained considering the electron–phonon interaction and the quantization of the acoustic phonon in the small wires. A different testing structure, using nanowires as the suspension for a heated island, was used by Schwab and coworkers [101]. They observed quantized conductance at 1 K. At slightly higher temperatures, their experimental data can only be explained by considering some diffuse scattering at the interfaces.

A different method for thermal conductivity characterization of one-dimensional structures was developed more recently by Shi and co-workers [99, 235]. Their idea is to use freestanding microfabricated structures (islands) whose temperature can be controlled and measured individually by thin-film resistors deposited onto the surface. The nanowire is then suspended between two islands and the thermal conductivity measurements are carried out by applying Joule heating to one of the islands, while the temperatures of both islands are monitored. Key challenges of this method include the minimization of the thermal contact resistance between the specimen and the microfabricated structure, and the maximization of the thermal resistance of the suspension structure. This method has been employed to measure the thermal conductivity of multiwalled carbon nanotubes and Si nanowires with various diameters [104].

The key challenge for the property measurement of nanowires lies in sample preparation, especially aligning electrodes to nanowires or nanowires to fabricated testing structures. So far, existing reports have relied on sophisticated micro- and nanofabrication techniques. There is a need for continued development of measurement techniques and more systematic study on the thermophysical properties of nanowires.

4.2. Temperature Measurement

In addition to thermophysical property characterization, measurements of temperature distributions are also of interest in many emerging technologies. The infrared thermal imaging techniques are limited to a resolution of a few micrometers, far from the resolution needed for thermal mapping in surrounding nanostructures. Several techniques

for thermal mapping at nanoscale have been proposed and are currently under development.

4.2.1. Scanning Thermal Microscopy

Scanning probe microscopes have provided nanoscale topographical resolution and it thus appears natural to locate a temperature sensor at the apex of the probes for thermal mapping. In fact, the first attempts in thermal mapping, after the invention of scanning tunneling microscope but before the birth of the atomic force microscope, was to use a thermocouple tip to measure surface topology of nonconducting surfaces according to conductance variation [236]. Several strategies have been proposed to place temperature sensors at the apex of AFM tips [237–239]. One method is to use a thermocouple as the cantilever and the other method is to place a thermistor at the apex. Both methods have gone through many improvements in the thermal sensor fabrication [240]. The estimated spatial resolution is 30–50 nm. One key issue with contact thermal mapping is the topology effect. Surface roughness changes the thermal contact resistance between the sample and the sensing tip. Low thermal conductance cantilevers have helped to minimize the heat flow from the sample to the cantilever, which reduces the topology effects on thermal imaging [235]. Also important to the accuracy of temperature estimation are the heat transfer mechanisms between the sample and the sharp tip [235]. Thermal images from scanning thermal microscopy (SThM) have provided new information for understanding the heat generation and heat conduction mechanisms in nanostructures. However, AFM based thermal imaging still has not reached the quantitative stage. An interesting theoretical question is what the resolution of SThM means since thermal transport around the SThM can be highly ballistic and nonequilibrium.

4.2.2. Near-Field Thermal Imaging

The near-field scanning optical microscope has the capability to break the optical diffraction limit [241]. In near-field infrared microscopy [242] similar probes have been used to obtain thermal images of 2 μm wide metal strips. The aperture diameter was of 1.5 μm, approximately one order of magnitude smaller than the dominant wavelength of thermal radiation at room temperature. A method to further increase the spatial resolution of the temperature measurement is to use visible radiation to probe the local change of reflectivity with temperature [243]. However, while the spatial resolution of near-field microscopy depends primarily on the aperture size, the low transmittance through the aperture probes drastically limits measurement sensitivity. This is even worse for thermal emission measurements due to the small thermal signal. One way to overcome this problem is to use solid-immersion lenses that could improve the spatial resolution without loss in sensitivity [244]. So far, near field thermal imaging has not reached the same level as SThM in terms of the image quality and resolution.

4.2.3. Thermal Reflectance Imaging

The photothermal method relies on the change of reflectance with temperature. This effect has been used extensively in the property measurements. Because the temperature dependence of the reflectance is generally small, $(10^{-4}–10^{-6})$/K, phase-locked detection schemes are often used, which requires periodic heating [224, 246]. For photothermal reflectance based property measurements, the periodic heating is realized by an external light source [224, 245]. For the thermal imaging of electronic devices, the devices are often biased with an ac current to periodically vary the temperature fields. Although such ac biasing may not correspond to the actual device operating conditions, the thermal mapping obtained leads to qualitative information on the hot spots. Transient heating has also been used, leading to an absolute measurement of the temperature distribution [247]. The thermal reflectance method can have a resolution of the order the laser wavelength used.

4.2.4. Raman and Luminescence Based Temperature Mapping

Raman spectroscopy measures the Stokes and the anti-Stokes shift of the laser line due to the phonon scattering of light. The intensity of the Stokes and the anti-Stokes lines depends on the phonon population and thus the temperature. From the intensity ratio of the two lines, the phonon temperature can be determined. Alternatively, the linewidth can also be used for temperature determination. Raman-based temperature mapping has been used in the investigation of the facet heating of semiconductor lasers [166, 248–250]. Similarly, photoluminescence peaks also depend on temperature and have been used for temperature mapping [251]. The advantage of the Raman spectroscopy method is that the ratio of the Stokes and the anti-Stokes line intensity depends on the phonon temperature only. However, the best temperature resolution reported so far is of the order of a few degrees.

5. ANALYTICAL TOOLS

The analysis and modeling of nanoscale heat transfer phenomena are challenging and complicated by several factors. One is that the mechanisms of nanoscale heat transfer are not well understood. Figure 6 shows different possible regimes of heat transfer. The determination of which regime a specific problem at hand falls into is nontrivial. Another major problem is that heat transfer rarely occurs only at nanoscale because eventually heat is dissipated into the macroscopic environment. Many heat transfer problems are multidimensional and multiscale spanning from nanoscale to macroscale. Tools for analyzing different problems are still evolving. In this section, we will divide our discussion into four directions: (1) purely ballistic transport, (2) classical size effects, (3) quantum size effects, and (4) multiscale modeling.

5.1. Purely Ballistic Transport

If all the geometrical length scales involved in the transport processes are much smaller than the energy carrier mean free path, the internal scattering of heat carriers can be completely neglected (i.e., transport is purely ballistic). An example is the radiation heat transfer in a vacuum enclosure, which is a topic in standard heat transfer textbooks.

The short mean free paths of electrons and phonons mean that this situation only occurs in nanostructures and very often at extremely low temperatures when the mean free path is long. Modeling of heat transfer in this purely ballistic limit is relatively simple. In thermal radiation, the concept of radiation shape factors is often used for heat transfer calculations. Typical radiation heat transfer treatment is limited to the incoherent regime where the phase information can be neglected. A more general formulation is the Landauer formalism that treats transport as a transmission process [252]. The energy transfer between two points in space is

$$\begin{aligned} q_{12} &= \frac{1}{8\pi^3}\sum_p\Big[\int E(k_1)v(k_1)\tau_{12}(k_1)f_0(T_{e1},E_{fe1})d^3k_1 \\ &\quad - \int E(k_2)v(k_2)\tau_{21}(k_2)f_0(T_{e2},E_{fe2})d^3k_2\Big] \\ &= \frac{1}{8\pi^3}\sum_p\Big[\int E(k_1)v(k_1)\tau_{12}(k_1)[f_0(T_{e1},E_{fe1}) \\ &\quad - f_0(T_{e2},E_{fe2})]d^3k_1\Big] \end{aligned} \tag{21}$$

where E is the energy per carrier, v is the carrier velocity, τ_{12} is the transmissivity from point 1 to point 2, k_1 are the wavevectors at point 1, f_0 is the distribution function, and the summation is over all polarizations of the heat carriers. We have used T_{e1}, E_{fe1} to emphasize that f_o represents the carriers leaving the point 1, not necessarily the local equilibrium temperature, as we discussed in Figure 8 for the thermal boundary resistance. The second equality of the Landauer formalism for heat flux comes from the principle of the detailed balance, which says that at equilibrium, there is no net flux.

Under the Landauer formalism, the key is to calculate the carrier transmissivity from point 1 to point 2. Both the wave and particle descriptions can be included under the Landauer formalism. In Section 2.1.1, for example, we discussed several models used to evaluate the phonon transmissivity across an interface and from the Landauer formalism, one can get the expression for the thermal boundary resistance of an interface expressed by Eq. (15). Similarly, the classical thermal radiation calculation based on the radiation shape factors can be understood as the calculation of the transmissivity. Landauer formalism can also be applied to obtain the universal thermal conductance of a nanowire, by considering the quatization of the energy spectrum of nanostructures [101]. Through the calculation of the transmissivity of acoustic waves and electromagnetic waves in layered structures, the Landauer formulation has been used to study the thermal conductance of superlattices and for radiation heat transfer across small spaces and for phonon heat conduction in thin films [28].

5.2. Classical Size Effects Regime

In Figure 6, we defined the classical size regime as the region when the mean free path is long compared to the characteristic length and when the scattering at the boundaries is strongly phase-breaking and randomizing. Under this situation, the energy spectrum of the heat carriers is close to that in bulk materials, with the complication that boundaries alter the trajectory of the heat carriers. We also grouped part of the quantum size regime as approximately treatable with the approaches for classical size effect described in this section. This occurs when the thermal wavelength is shorter than the domain size, but as explained in Section 2.1, this approximation does not always work and should be used prudently. In the classical size regime, the major new physics in addition to transport in bulk materials is the boundary scattering. This is a conceptually relatively easy addition. Commonly used tools for dealing with such size effects are the Boltzmann equation and Monte Carlo simulation.

5.2.1. Boltzmann Equation Approach

The Boltzmann transport equation (BTE) applies to dilute particles such as gas molecules, electrons, phonons, and photons. In its general form, the BTE can be written as [19]

$$\frac{\partial f}{\partial t} + \mathbf{v}\cdot\nabla_{\mathbf{r}}f + \mathbf{F}\cdot\nabla_{\mathbf{p}}f = \left(\frac{\partial f}{\partial t}\right)_c \tag{22}$$

where f is the statistical distribution function of an ensemble of carriers, which depends on time t, position vector $\mathbf{r}$, and momentum vector $\mathbf{p}$. $\mathbf{F}$ is the force vector applied to the particles. The key to the Boltzmann equation is the scattering term, which is the term that restores the system to equilibrium. Quantum mechanical principles are often used to deal with scattering. The perturbation treatment in quantum mechanics leads to the Fermi golden rule of calculating the scattering probability from one quantum state to another. A general expression of the scattering integral can be formally written based on the scattering probability and the distribution function [19]. This leads to an integral-differential form of the Boltzmann equation which is difficult to solve but has often been treated in thermal radiation transport in the form of equation of radiative transfer [25, 253]. For phonon and electron transport, as well as gas transport, the relaxation time approximation is often used,

$$\left(\frac{\partial f}{\partial t}\right)_c = \frac{f_0 - f}{\tau(\mathbf{r},\mathbf{p})} \tag{23}$$

where f_0 is the equilibrium distribution (i.e., Fermi–Dirac distribution for electrons, Bose–Einstein distribution for phonons, and Maxwell–Boltzmann distribution for gas molecules) and $\tau(\mathbf{r},\mathbf{p})$ is the relaxation time as a function of position and momentum and is often approximated as energy-dependent rather than wavevector-dependent [254]. When multiple scattering coexists, for example, carrier–carrier scattering and carrier–impurity scattering, the Mathessien rule is often used to obtain the total relaxation time [19].

There are two different approaches to deal with the boundary scattering of nanostructures on transport processes. One is to add an extra boundary scattering term into the relaxation time through the Mathiessen rule [19]. This approach is simple and has been widely used in dealing with low temperature transport problems in bulk materials where size effects are important, but it is not accurate because while carrier–carrier scattering and carrier–impurity scattering are volumetric processes, interface scattering occurs at

the surfaces [255]. The other approach is to treat interfaces and boundaries through boundary conditions to the Boltzmann equation. In this latter approach, the relaxation time in bulk materials without any size effects is first determined. The effects of the interfaces and boundaries of nanostructures are imposed as the boundary conditions.

Classical size effects on transport processes and properties of all the energy carriers have been studied in the past. The classical size effects on electron transport were summarized in the book of Tellier and Tosser [56]. Flow and heat transfer of rarefied gas has also been studied extensively in the past [256]. Size effects on phonon transport started in the 1930s through Casimir's pioneering work [257]. The last two decades have seen a surge of investigations on phonon size effects in low-dimensional structures [11, 12].

The most studied phonon size effect is the thermal conductivity reduction in thin films. Phonon heat conduction in thin silicon thin films has been measured and modeled by Volklein and co-workers on polycrystalline thin films for thermoelectric applications [258, 259] and by Goodson and Ju for single crystalline silicon thin films [3, 22]. The modeling for the in-plane thermal conductivity of single crystalline thin films is a simple extension of the Fuchs and Sonderheim classical treatment of the electron size effects [67, 260, 261]. For polycrystalline films, the gray boundary scattering adds another relaxation time that has been grouped into the bulk relaxation time according to the Mathiessen rule. A model based on geometrical consideration rather than solving the Boltzmann equation was developed by Flik and Tien [262]. Heat conduction perpendicular to a thin film was dealt with in several papers [46, 260–265]. Majumdar [263] solved the phonon Boltzmann equation assuming that the two surfaces of the film are black phonon emitters. Chen and Tien [260] developed a model for the thermal conductivity of quantum wells based on the BTE for both the in-plane and the cross-plane directions. The in-plane thermal conductivity is based on Fuchs' solution [54] while the cross-plane direction is based on the approximate solution developed for the photon transfer equation.

Size effects in multilayer structures are more difficult to model than a single layer. The incoherent particle transport models for thermal transport in superlattices based on the Boltzmann transport equation were developed by Chen and co-workers in a series of papers for transport in both in-plane and cross-plane directions [21, 48, 93] and by Hyldgaard and Mahan for the in-plane direction [20]. The models by Chen and co-workers assume partially diffuse and partially specular interfaces, with the fraction of specular interface scattering left as a fitting parameter. Figure 15a and b shows examples of the model fitting with experimental data for both in-plane and cross-plane directions. The experimental data are from Yao [79], Yu et al. [266], and Lee et al. [50]. The good agreement seems to indicate that the phase-breaking scattering processes dominate.

The Boltzmann equation approach as has been used in thin films and superlattices can be readily extended to one-dimensional structures, such as nanowires [102, 105]. Walkauskas et al. [106] solved the Boltzmann equation for square nanowires and compared the thermal conductivity of nanowires to thin films. As expected, additional lateral surfaces cause a more pronounced reduction in the thermal

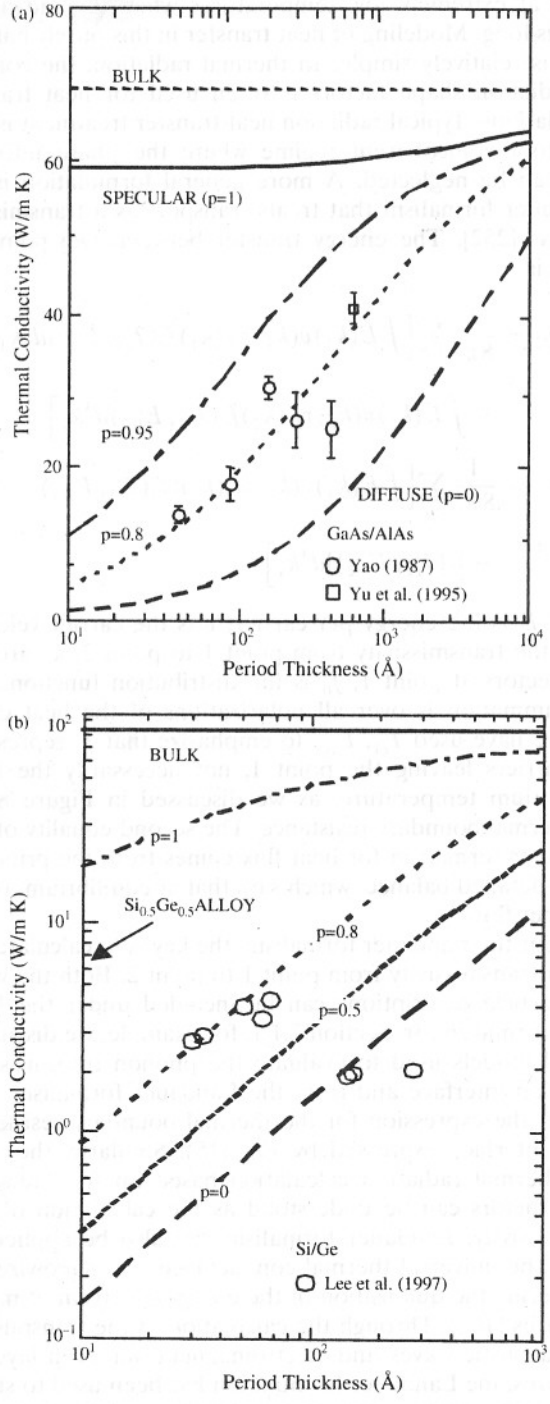

Figure 15. Modeled thermal conductivity of superlattices. (a) In-plane for GaAs–AlAs supperlattices. Reprinted with permission from [21], G. Chen, *Trans. ASME, J. Heat Transf.* 119, 220 (1997). © 1997, American Society of Mechanical Engineers. (b) Cross-plane for Si–Ge superlattices based on the Boltzmann equation. Reprinted with permission from [48], G. Chen, *Phys. Rev. B* **57**, 14958 (1998). © 1998, American Physical Society. The experimental data by Yao [79], Yu et al. [266], and Lee et al. [50] are also plotted.

conductivity of wires compared to films. Nanowire superlattices have also been modeled recently [45].

There have been many modeling studies in the past on the thermal conductivity of porous materials due to their applications in thermal insulation [267]. These models, however, cannot be applied to nanoporous materials because they did not include size effects, as is clearly required from experimental data [268]. Several attempts to include the size effects have been made in the modeling of the thermal conductivity of nanoporous silicon [269–271] and opals [272]. Size effects on nanocomposite thermal conductivity have been considered based on the inclusion of thermal boundary resistance [273]. One major difficulty in the Boltzmann equation approach lies in the solution of the equation. The Boltzmann equation is a phase space equation with seven variables. Direct numerical solution is generally difficult. There have been a few treatments applying the Boltzmann equation to nonplanar geometries that are more relevant to actual device configurations [117, 274]. More detailed discussion will be given in Section 5.4.

5.2.2. Monte Carlo Simulation

Monte Carlo simulation solves the Boltzmann transport equation in a statistical framework. Over the last decade or so, there has been tremendous advancement in the development of Monte Carlo solution techniques for the radiative transfer equation and the Boltzmann equation for electrons and holes in semiconductors [275–280]. Only a few reports using Monte Carlo technique for phonon transport have been published in the past. Peterson [281] employed the Monte Carlo method to simulate phonon transport in a confined space while Klitsner et al. [282] performed Monte Carlo simulations to obtain temperature distribution in a crystal. More recently Mazumder and Majumdar [283] considered phonon dispersion as well as various phonon scattering mechanisms to study heat transport in complex geometries and to predict the thermal conductivities. The result showed that by fitting one parameter using experimental data of thermal conductivity at one temperature, predictions of the thermal conductivity of silicon agree well experimental data over wide temperature range. In addition, it was able to capture both the ballistic and diffusive limits. The major advantage of this method is that the simulation code can be easily adapted to complex geometries. In addition, Monte Carlo simulation can separately treat various scattering mechanisms. The major disadvantage of the Monte Carlo method is its slow speed.

5.3. Quantum Size Effect Regime with Scattering

While it is relatively straightforward to treat wave effects if no scattering exists, the physical picture becomes less clear and mathematical treatment becomes more complicated when both wave effects and scattering coexist. If there is no scattering and the detailed geometries and atomic compositions of the nanostructures, particularly the interface structures, are known, the energy states of the nanostructures can be solved from the Schrödinger equation. Examples are the electron and phonon energy states of a perfect thin film or quantum well. The existence of internal scattering, however, usually distorts the energy states from these ideal calculations. Imperfect interface structures, which are usually unknown, further add to the complexity. The quantum form of the Boltzmann equation does exist [284]; similarly, quantum Green's function methods may also be applicable for treating nanoscale heat conduction problems [285]. None of these approaches, however, have been implemented so far for realistic nanostructures. So far, all the treatments for situations when both wave and scattering are in existence are all based on various assumptions that may be valid under certain conditions. There are two approximation strategies. One approach, for example, is to assume that the quantized energy states form first, usually calculated under perfect interface conditions. These quantized states are then treated as particles based on the Boltzmann equation. We will call this quantized incoherent transport. Clearly, whether this approximation is valid or not depends on the strength of the boundary scattering in breaking or randomizing the phases.

In this section, we will discuss several approaches that include, to a certain extent, the wave mechanisms, including (1) quantized incoherent transport, (2) the molecular dynamics simulation, and (3) the fluctuation–dissipation theorem approach.

5.3.1. Quantized Incoherent Transport

The quantized incoherent transport first computes the energy spectrum of the nanostructures. The subsequent motion of these quantized energy carriers, however, is treated as incoherent. Representation treatments include electron transport in quantum wells and quantum wires for thermoelectric energy transport studies [30, 178]. Electron energy states are quantized due to lateral confinement. Transport along the film plane or wire axis, however, is diffusive, either due to interface scattering or internal scattering. Experimental measurements of the electrical conductivity of nanowires seem to validate such an approach [286, 287].

For phonon heat conduction in thin films, nanowires, and superlattices, a similar approach has also been taken [58, 59]. The phonon spectra of nanowires and thin films have been computed based on continuum acoustic wave equations or the lattice dynamics method. For heat conduction along the film plane or wire axis, the assumption of a perfect interface does not lead to much change in the thermal conductivity compared to bulk materials [57]. This is also anticipated from a pure particle-based approach because in these cases, the structures simply act as waveguides [54, 55]. Only when diffuse interface scattering is included can these approaches lead to thermal conductivity predictions that are comparable to experimental observations. However, it is not clear at this stage whether such quantized states do form or not, and if yes, as some Raman spectroscopy would suggest [288] there is no quantitative information on the fraction of the quantized states compared to the bulk states.

Phonon heat conduction in superlattices offers another test to the assumption of a quantized incoherent transport model. Different lattice dynamics models have been used to compute the phonon spectra in various superlattices and these spectra are used to calculate the phonon group

velocity [88–90]. The Boltzmann equation is used to calculate the thermal conductivity using the new group velocity and the phonon density of states, assuming that the relaxation time of the superlattices is equal to that of its parent materials. These attempts, however, have not lead to quantitative agreement with experimental results, and in fact, even the qualitative agreement is poor as the lattice dynamics would lead to the thermal conductivity decreasing with period and eventually to a flat thermal conductivity that does not change with period. Figure 16 compares the lattice dynamics result with experimental results and clearly shows that neither the absolute values nor the trends are consistent with experimental data in both in-plane and cross-plane directions [51], except in the very thin period limit where the slight recovery of experimental thermal conductivity in some superlattices seems to agree with the trends of lattice dynamics predictions. In comparison, the incoherent transport models based on the assumption that phase coherence is not important leads to results that are in agreement with experimental data, particularly in the thick period regime [48, 93], as shown in Figure 15. This does seem to suggest that the phonon heat conduction processes in thin films are dominated by incoherent transport.

Why do bulk crystal solids form phonon band structures that can be used in the Boltzmann equation calculation, while the phonon band structure-based calculation for ideal superlattices seems to fail to explain the thermal conductivity? To answer this question, we can use the wave method to calculate how many layers are required to form the superlattice spectra that assume an infinite number of layers. Transfer matrix based calculation shows that 10 periods will suffice. Thus, phonons must remain phase coherent over such periods to form new superlattice bands. If diffuse interface scattering randomizes the phase, the calculated phonon

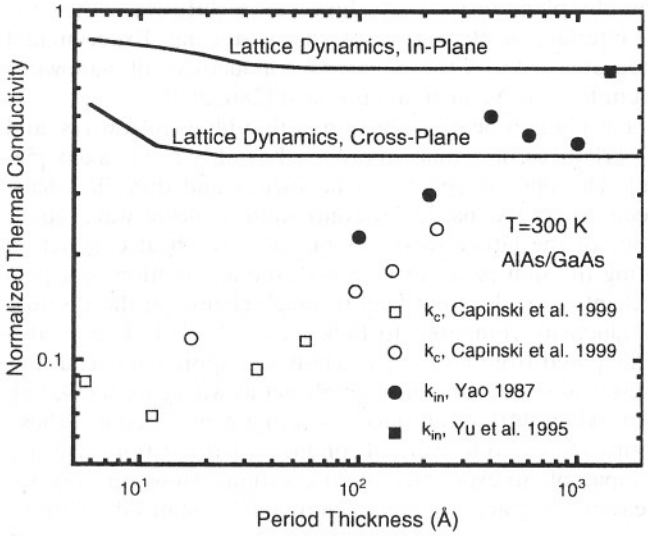

Figure 16. Comparison of lattice dynamics with experimental data. The experimental data are from Yao [79], Yu et al. [266], and Capinski et al. [80]. Adapted with permission from [51], B. Yang and G. Chen, in "Chemistry, Physics, and Materials Science for Thermoelectric Materials: Beyond Bismuth Telluride" (M. G. Kanatzidis, T. P. Hogan, and S. D. Mahanti, Eds.). Kluwer Academic/Plenum, New York, 2003. © 2003, Kluwer Academic/Plenum.

spectrum based on ideal interfaces is not valid and no superlattice mode or only partial modes form. In addition, internal scattering can also destroy the phases because 10 periods can be much longer than the phonon mean free path.

One way to treat both the quantized and the bulk energy states is to introduce an imaginary wavevector into the Bloch wave functions. When the imaginary wavevector is large, the waves are highly damped and only sample few unit cells of the original crystals making up the nanostructrure and thus tend to recover to the bulk dispersion. When the imaginary wavevector is zero, the lattice waves extend over the whole structure and the new energy bands will form. The method was first used by Pendry for electron transport [289]. Simkin and Mahan introduced it to lattice dynamics for calculating superlattice thermal conductivity [290]. Their model is able to predict a minimum in the cross-plane thermal conductivity and the period dependence. However, the Simkin and Mahan model does not consider the diffusive interface scattering, which is probably one major cause of the reduced mean free path in superlattices. As a consequence, their model cannot explain the in-plane thermal conductivity reduction in superlattices, nor the absolute magnitude of thermal conductivity reduction in the cross-plane direction. Yang and Chen related the imaginary wavevector to the interface diffuse scattering [51, 291]. This approach enables the calculation of the thermal conductivity of superlattices in both in-plane and cross-plane directions, both leading to good agreement with experimental data, as shown in Figure 17.

5.3.2. Molecular Dynamics Simulation

Like lattice dynamics, classical molecular dynamics (MD) simulation also solves Newton's second law to track the motion of all atoms in a system [292–294]. The difference between lattice dynamics and molecular dynamics is that lattice dynamics uses harmonic forces while molecular dynamics inputs the true potential of atomic interaction. Bolstered by advances in computation power, MD has become a powerful tool for studying material formation processes and material properties and it is increasingly employed to study heat transfer [295–306]. Its key limitations are determination of accurate potentials and the size of systems that can be studied. Fortunately well-tested empirical potential are available for most of the material of interest. For example the Stillinger–Webber potential is often used for silicon [307]. System size is currently the greatest limitation. Recent large-scale MD simulations of fluid flows involve ~200,000 atoms and solids of 10–100 million atoms depending on necessary times of simulation [308, 309]. Unfortunately, the mean free path of heat-carrying phonons in silicon crystals is ~3000 Å [3, 48]; yet even a 1000 Å on a side cube of silicon contains ~50 million atoms and requires a long run time to accumulate phonon statistics.

Equilibrium and nonequilibrium MD simulations have been used in heat transfer studies. In the nonequilibrium approach, a temperature difference or energy flux is imposed by altering the atomic dynamics in localized boundary regions [310, 311]. In general, nonequilibrium techniques suffer from three major drawbacks: (1) the simulation

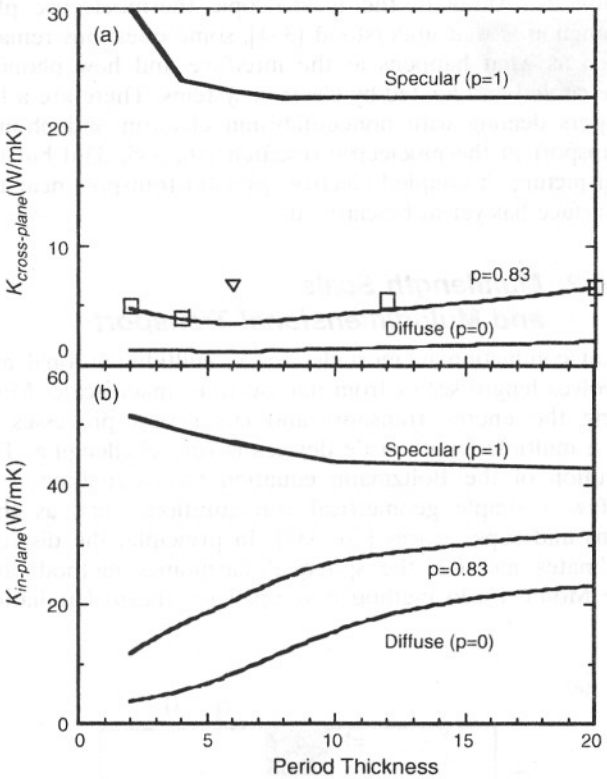

Figure 17. Thermal conductivity of GaAs/AlAs superlattices obtained from incoporating diffuse interface scattering into a lattice dynamics model; experimental data from Capinski et al. [80] are also plotted. Adapted with permission from [51], B. Yang and G. Chen, in "Chemistry, Physics, and Materials Science for Thermoelectric Materials: Beyond Bismuth Telluride" (M. G. Kanatzidis, T. P. Hogan, and S. D. Mahanti, Eds.). Kluwer Academic/Plenum, New York, 2003. © 2003, Kluwer Academic/Plenum.

domain must contain enough atoms in the boundary regions to stabilize the boundary temperatures, which increases the overall cost of the simulation; (2) the systems that can be simulated are smaller than the phonon mean free path and their small size also restricts the maximum phonon wavelength; and (3) an unphysically large temperature gradient is required to converge temperature statistics, making it difficult to determine the thermal conductivity at a particular temperature. So far, the nonequilibrium MD simulation techniques have been applied to thin films, nanowires, and carbon nanotubes [112, 301, 312].

The equilibrium approach relies on small statistical temperature fluctuations to drive instantaneous heat fluxes [313–315]. Although the time average of this heat flux vanishes, the thermal conductivity of the system to the disturbance can be calculated from the instantaneous heat flux autocorrelation function according to the Green–Kubo formula [314]. Convergence is slow, but the equilibrium approach is free of the three drawbacks associated with the nonequilibrium technique (periodic boundary conditions effectively remove the mean free path limitation [301, 303]), although care still must be taken to avoid artificial size effects of the finite simulation domain. Equilibrium methods have been used to diagnose the thermal conductivity of many materials including recent computations of high thermal conductivity materials such as silicon and diamond [301, 302]. The MD simulation of thermal conductivity of superlattices has also been explored [316–319]. Recently, Daly and co-workers used MD simulation to investigate the effects of interface mixing on the thermal conductivity in GaAs/AlAs superlattices [70]. Their simulations show that for perfect interface, the results are similar to that of lattice dynamics. For the case of superlattices with interface mixing, the simulation results are much closer to experimental data, further reinforcing the discussion we had previously on the heat conduction mechanisms in superlattices.

From the time history of individual atoms in a MD simulation, phonon spectral characteristics can be analyzed by discrete Fourier methods. Thus the relaxation time and other important properties such as phonon spectrum, group velocity, and density of states can be computed from the time history of the atomic trajectory and its velocity [320]. In principle, such information can be incorporated into the Boltzmann equation to treat heat transfer mesoscale systems that cannot be simulated directly by the MD methods. In addition, MD simulation can be the most ideal tool to study the imperfect interface and anharmonic scattering while lattice dynamics or acoustic modeling can only model the process qualitatively by assuming idealized interfaces and neglecting all anharmonic scattering in nanostructures. Some MD studies have examined thermal boundary resistance [321–324].

One theoretical drawback of the classical MD method is that it does not include the quantum statistics and quantum scattering mechanism. Such a drawback limits the MD results to high temperatures when the quantum effects are negligible. There have also been theoretical attempts to correct the difference between quantum and classical simulations. The first correction is on the temperature. Other modeling suggests that quantum effects on scattering are not large. This topic, however, needs further study.

5.3.3. Fluctuation–Dissipation Theorem Based Wave Approach

A well-established method to treat both the absorption, emission, and wave effects in thermal radiation is the fluctuaction–dissipation theorem based approach established by Rytov [325]. This approach was used to formulate the problem of radiation heat transfer between two closely spaced surfaces [14], radiative transfer in absorbing and emitting thin films [326], and recently was used for treating radiation exchange between surfaces due to surface modes [147, 151]. In this approach, the emission is related to the fluctuation of microscopic current sources, the strength of which is related to the local temperature through the fluctuation–dissipation theorem. The propagation of the electromagnetic field generated by each current source is solved based on the Maxwell equations. This approach, in theory, can be extended to acoustic waves and maybe even electron waves, but no such attempts have been reported.

5.4. Multicarrier and Multidimensional Transport

Heat transfer and energy conversion in electronic and thermoelectric devices often involve multicarriers and multiple length scales. For example, heat is typically generated in a nanometer-scale region at the drain of a MOSFET when hot electrons relax their energy to phonons and is subsequently conducted through the millimeter thick substrate to the surroundings. In this section, we will discuss the modeling of nonequilibrium electron and phonon transport and the multidimensional transport problems.

5.4.1. Coupled Electron–Phonon Transport

Traditionally, it is assumed that electrons and phonons are under local equilibrium in modeling transport phenomena in a solid. However, the equilibrium between electrons and phonons can be disrupted in many cases. For example, in the presence of a sufficiently high electric field, electrons can be energized and thrown far out of equilibrium from phonons [127]. This is termed the hot electron effect. Such a nonequilibrium condition becomes important for microelectronic devices because the electric fields become higher as the feature size shrinks. In the case of laser–material interactions, the electrons can be thrown out of equilibrium from lattice due to excitation by ultrashort laser pulses [126, 327].

For coupled electron and phonon transport in nanostructures, the electron and phonon Boltzmann equations should be solved simultaneously. This approach, however, has not been taken due to the numerical complexity involved. In the past, the electron hydrodynamic equations are often used for modeling electron transport for practical device simulation, coupled to the diffusion treatment for the phonon heat conduction [328–331]. The hydrodynamic equations assume that electrons and phonons are in local equilibrium with their own pools. In a quite similar way, Qiu and Tien studied conversion and transport phenomena during ultrafast processes such as femtosecond to nanosecond laser–material interactions based on treating electrons and phonons as separate systems [126, 332]. Their theoretical and experimental studies show that it is the nonequilibrium nature between electrons and phonons during the femtosecond laser–metal interactions, rather than the hyperbolic heat conduction effect, that dominates the observed experimental phenomena. However, in these models, the ballistic transports are not counted, neither for electrons nor for phonons. Sometimes the electron transport is solved from the full-blown Boltzmann equation or Monte–Carlo simulation to count the ballistic nature of electrons [333]. However, very little work has been done to study the effect of ballistic phonon transport on electron transport. Concurrent modeling of the nonequilibrium electron and phonon transport based Boltzmann equation is desirable.

Along the same line, the coupled electron–phonon transport is the basis for solid-state energy conversion such as thermoelectric and thermionic cooling and power generation. Taking thermoelectric cooling as an example, electrons take energy away from phonons at a metal–semiconductor interface, carrying it to the hot side, and rejecting it to phonons. Although the macroscopic thermoelectric phenomenon is well understood [334], some questions remain, such as what happens at the interface and how phonons are cooled and heated by electron systems. There are a few papers dealing with nonequilibrium electron and phonon transport in thermoelectric research [46, 335, 336] but the full picture of coupled electron–phonon transport near the interface has yet to be clarified.

5.4.2. Multilength Scale and Multidimensional Transport

Heat conduction in most devices is multidimensional and involves length scales from nanoscale to macroscale. Modeling the energy transport and conversion processes in such multiple length scale devices is very challenging. The solution of the Boltzmann equation has been limited to a few a simple geometrical configurations such as thin films and superlattices [76, 337]. In principle, the discrete ordinates method, the spherical harmonics method, and the Monte Carlo method developed for thermal radiation

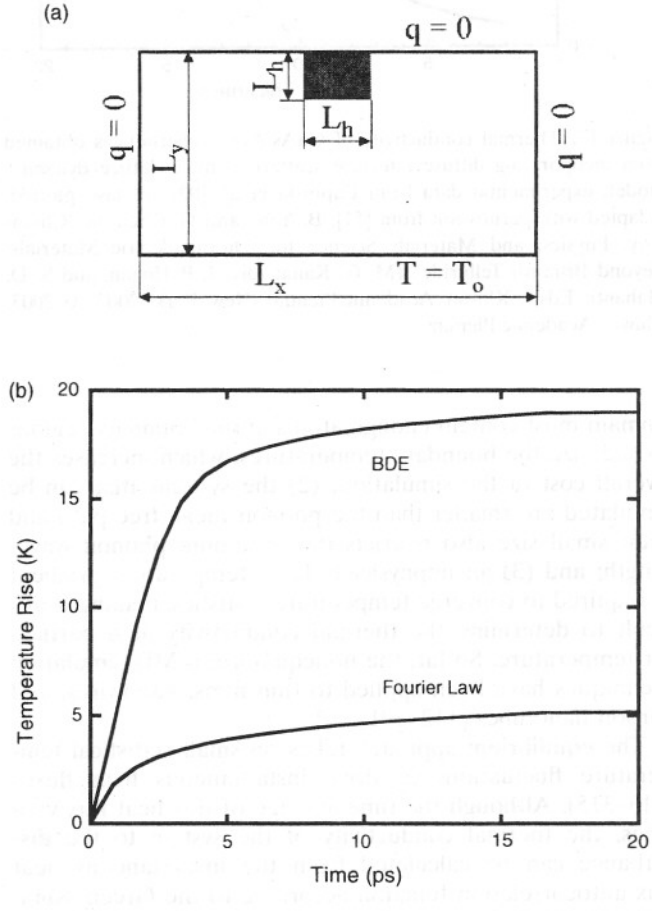

Figure 18. Comparison of the peak temperature rise of nanoscale heat source. (a) a 10 nm × 10 nm ×1μm hot strip embedded in the silicon substrate and (b) the peak temperature predicted by the Fourier law is much smaller than that predicted by the ballistic–diffusive equations. Reprinted with permission from [121], R. G. Yang, et al., in "Proceedings of the 12th International Heat Transfer Conference" (J. Taine, Ed.), Vol. 1, pp. 579–584. Elsevier, Paris, 2002. © 2002, Elsevier.

[253] can be used to solve the Boltzmann transport equation. However, fewer studies have gone beyond nonplanar and multidimensional geometries [117, 120, 121, 271, 283, 338, 339].

Direct numerical solution of the Boltzmann equation, however, is usually slow. Approximate methods that are capable of capturing the major size effects but easier to implement are thus desirable. One such method, for example, is to focus on the interface region only by introducing appropriate boundary conditions, while away from the boundaries the usual diffusion or drift-diffusion equations are used. Examples are the velocity slip boundary condition for rarefied gas flow [256] and the Deissler temperature jump boundary condition for photon radiation heat transfer [25]. Similar interface conditions, called diffusion–transmission interface conditions, have been introduced for phonon and electron transport [340].

Another approximation that provides further improvements compared to the introduction of special interface conditions is to split the carriers inside the medium into two groups—a ballistic component and a diffusive component. The ballistic component originating from boundaries and nanoscale heat sources experiences outscattering only. This group can be explicitly solved through a path integral. The transport of the scattered and excited heat carriers is treated as a diffusive component with the diffusion approximation. This approach was first used for thermal radiation [253] and was recently employed by Chen to develop the ballistic–diffusive heat conduction equations. Yang et al. [121, 338] applied the ballistic–diffusive equations to study the phonon rarefaction effect, the heat transfer surrounding a nanoscale heat source. The heat source is similar to the phonon hot spot generated in a MOSFET device. A 10 nm × 10 nm × 1μm hot strip is embedded in the silicon substrate (Fig. 18a). The power generation rate is 1×10^{19} W/m^3, typically for a period of ~10 ps. Figure 18b shows the highest temperature rise in the device as a function of time. Both Fourier law and ballistic–diffusive equations predict a saturation temperature rise after 10 ps. The peak temperature predicted by the Fourier law is much smaller than that predicted by the ballistic–diffusive equation, due to the rarefied phonon heat conduction effect discussed in Section 3. The experiment by Sverdrup and co-workers [123] also demonstrates such a phonon rarefaction effect.

6. SUMMARY

In this chapter, we discussed the uniqueness of heat transfer phenomena in nanostructures. Figure 6 summarizes different heat transfer regimes that one may encounter at nanoscale. When the structure characteristic lengths are comparable to the mean free path, size effects become important. In the classical size effect regime, the phase of the energy carriers can be neglected while it must be included in the quantum size effect regime. The distinction between the classical and the quantum size effect regime depends on the phase-breaking strength of the interface scattering processes, which is not well understood now. Thermal wavelength provides another length scale to judge whether the bulk energy spectrum is a good approximation. This length scale, however, must be used carefully because although the average energy spectrum does not change much when the structure is much larger than the thermal wavelength, the group velocity in specific transport directions can have significant changes, as in the case of superlattices. Some examples of nanoscale heat transfer phenomena in the quantum regime include interference, tunneling, and even coherent thermal emission. In the classical size effect regime, diffuse interface scattering tends to reduce the heat transfer through the system.

Nanoscale heat transfer phenomena can have significant implications for a variety of contemporary technologies, some undesirable as the classical size effects on the thermal management of microelectronics and optoelectronic devices, while others can be utilized to improve the data storage density or energy conversion efficiency, as in thermoelectric cooling and power generation and in thermophotovoltaic energy conversion. Nanoscale heat transfer is also related to nanomaterial synthesis and nanofabrication and some emerging biotechnologies.

Experimental and modeling tools for nanoscale heat transfer are discussed. Various measurement techniques have been developed in the past for the thermophysical property determination of thin films and superlattices. Experimental techniques for characterizing nanowires and other nanostructures, such as nanowires and nanoparticles, still need further development. Impressive progresss has been made in thermal imaging at nanoscale based on the scanning probe microscope but the technique has stayed mainly at a qualitative level. With regard to modeling, the classical size effects region and purely ballistic transport regimes can be treated reasonably well. Key challenges exist for the regime when both wave effects and scattering coexist because scattering can change the energy spectrum of nanostructures. At room temperature, experimental studies so far suggest that phonon transport falls mostly into the classical size effect regime while electron transport can fall into the quantized incoherent transport regime. From the discussions, it is clear that much work remains to be done in both experimental and modeling arenas.

GLOSSARY

Acoustic phonons The lower branches of phonon modes in the dispersion curves.

Blackbody radiation The radiation emitted by a blackbody. A blackbody is a virtual object that absorbs all radiation incidents on it.

Dispersion relation Relates the frequency of a carrier, ω_k, to its wavevector k. The *group velocity* of the carrier can be found from the dispersion relation through $v_k = \frac{\partial \omega_k}{\partial k}$.

Elastic scattering There is no net change of energy of each involved particle before and after an elastic scattering process.

Inelastic scattering The energy of some of participating carriers changes before and after an inelastic scattering process. Refer to elastic scattering.

Mean free path The average distance a particle moves between succesive collisions.

Optical phonons The upper branches of phonon modes in the dispersion curves, refer to acoustic phonons.

Phonons Quanta of lattice waves in solids.

Phonon-polariton The hybrid mode of the coupled phonon and electromagnetic transverse wave field.

Phonon rarefaction Occurs when the heating/cooling region is much smaller than the phonon mean free path.

Stokes/Anti-Stokes shift Represents a change in energy (frequency) of photon scattered by a substance due to photon-phonon interaction. The scattered photon may have a smaller frequency (Stokes shift) or higher frequency (anti-Stokes shift) depending whether a phonon has been generated or absorbed during the scattering process.

Thermal boundary resistance or Kapitza resistance Used to describe the additional thermal resistance due to the reflection of energy carriers at an interface when the heat transports across the interface.

ACKNOWLEDGMENTS

The authors are grateful to M. S. Dresselhaus and members of the Nanoengineering Group at MIT Rohsenow Heat Transfer Lab for stimulating discussions. G.C. gratefully acknowledges the support of NSF (CTS-0129088), DOE (DE-FG-02ER45977), ONR MURI on Thermoelectrics, and ONR MURI on Electromagnetic Metamaterials through UCLA, and by Draper Lab.

REFERENCES

1. C.-L. Tien, A. Majumdar, and F. M. Gerner, "Microscale Energy Transport." Taylor & Francis, Washington, 1998.
2. G. Chen, "Nanoscale Heat Transfer and Energy Conversion." Oxford Univ. Press, in press.
3. K. E. Goodson and Y. S. Ju, *Annu. Rev. Mater. Sci.* 29, 261 (1999).
4. G. Chen, *Annu. Rev. Heat Transf.* 7, 69 (1996).
5. T. Tritt, "Recent Trends in Thermoelectric Materials Research," Semiconductors and Semimetals Series, Vol. 69–71. Academic Press, San Diego, 2001.
6. G. Chen and A. Shakouri, *Trans. ASME, J. Heat Transf.* 124, 242 (2002).
7. R. S. DiMatteo, P. Greiff, S. L. Finberg, K. Young-Waithe, H. K. H. Choy, M. M. Masaki, and C. G. Fonstad, *Appl. Phys. Lett.* **79**, 1894 (2001).
8. G. Binning, M. Despont, U. Drechsler, W. Häberle, M. Lutwyche, P. Vettiger, H. J. Mamin, B. W. Choi, and T. W. Kenny, *Appl. Phys. Lett.* 74, 1329 (1999).
9. M. I. Flik, B. I. Choi, and K. E. Goodson, *Trans. ASME, J. Heat Transf.* 114, 667 (1992).
10. C. L. Tien and G. Chen, *Trans. ASME, J. Heat Transf.* **116**, 799 (1994).
11. G. Chen, "Semiconductors and Semimetals," Vol. 71, p. 203. Academic Press, San Diego, 2001.
12. D. G. Cahill, W. K. Ford, K. E. Goodson, G. D. Mahan, A. Majumdar, H. J. Maris, and R. Merlin, *J. Appl. Phys.* 93, 743 (2003).
13. G. A. Domoto, R. F. Boehm, and C. L. Tien, *Trans. ASME, J. Heat Transf.* 92, 412 (1972).
14. D. Polder and M. Von Hove, *Phys. Rev.* 4, 3303 (1971).
15. F. P. Incropera and D. P. DeWitt, "Fundamentals of Heat and Mass Transfer," 5th ed. Wiley, New York, 2002.
16. C. Kittel, "Introduction to Solid State Physics," 7th ed. Wiley, New York, 1996.
17. N. W. Aschroft, and N. D. Mermin, "Solid State Physics." Sauders, Forth Worth, PA, 1976.
18. R. Berman, "Thermal Conduction in Solids." Clarendon, Oxford, 1976.
19. J. M. Ziman, "Electrons and Phonons." Clarendon, Oxford, 1960.
20. P. Hyldgaard and G. D. Mahan, "Thermal Conductivity." Technomic, Lancaster, UK, 1996.
21. G. Chen, *Trans. ASME, J. Heat Transf.* 119, 220 (1997).
22. Y. S. Ju and K. E. Goodson, *Appl. Phys. Lett.* 74, 3005 (1999).
23. D. K. Ferry and S. M. Goodnick, "Transport in Nanostructures." Cambridge Univ. Press, Cambridge, UK, 1999.
24. M. Born and E. Wolf, "Principles of Optics," 6th ed. Pergamon Press, Oxford, 1980.
25. R. Siegel and J. R. Howell, "Thermal Radiation Heat Transfer." Hemisphere, Washington, 1992.
26. C. L. Mehta, *Nuovo Cimento* 21, 401 (1963).
27. G. Chen and C. L. Tien, *Trans. ASME, J. Heat Transf.* 114, 636 (1992).
28. G. Chen, *Trans. ASME, J. Heat Transf.* 121, 945 (1999).
29. S. Schaaf, and P. Chambre, "Flow of Rarefied Gases." Princeton Univ. Press, Princeton, NJ, 1961.
30. L. D. Hicks and M. S. Dresselhaus, *Phys. Rev. B* 47, 16631 (1993).
31. M. S. Dresselhaus, Y. M. Lin, S. B. Cronin, O. Rabin, M. R. Black, G. Dresselhaus, and T. Koga, "Semiconductors and Semimetals," Vol. 71, p. 1. Academic Press, San Diego, 2001.
32. B. Yang and G. Chen, *Microscale Thermophys. Eng.* 5, 107 (2001).
33. H. Raether, "Surface Plasmons." Springer-Verlag, Berlin, 1998.
34. D. L. Mills and E. Burnstein, *Rep. Progr. Phys.* 37, 817 (1974).
35. C. K. Campbell, "Surface Acoustic Wave Devices for Mobile and Wireless Communications." Academic Press, San Diego, 1998.
36. J. Grefett, R. Carminati, K. Joulain, J.-P. Mulet, S. Malnguy, and Y. Chen, *Nature* 416, 61 (2002).
37. R. Hillenbrand, T. Taubner, and F. Keilmann, *Nature* 418, 159 (2002)
38. L. Esaki and R. Tsu, *IBM J. Res. Dev.* 14, 61 (1970).
39. C. Weisbuch and B. Vinter, "Quantum Semiconductor Structures: Fundamentals and Applications." Academic Press, Boston, 1991.
40. E. Yablonovitch, *Phys. Rev. Lett.* 58, 2059 (1986).
41. J. Joannapoulos, R. D. Meade, and J. N. Winn, "Photonic Crystals." Princeton Univ. Press, Princeton, NJ 1995.
42. E. T. Swartz and R. O. Pohl, *Rev. Mod. Phys.* 61, 605 (1989).
43. P. L. Kapitza, *Zh. Eksp. Teor. Fiz.* 11, 1 (1941) [*J. Phys. (USSR)* 4, 181 (1941)]; in "Collected Papers of P. L. Kapitza" (D. der Haar, Ed.), Vol. 2, p. 581. Pergamon, Oxford, 1965.
44. W. A. Little, *Can. J. Phys.* 37, 334 (1959).
45. C. Dames and G. Chen, *J. Appl. Phys.* 95, 682 (2004).
46. G. Chen and T. Zeng, *Microscale Thermophys. Eng.* 5, 71 (2001).
47. J. A. Katerberg, C. L. Reynolds, Jr., and A. C. Anderson, *Phys. Rev. B* 16, 673 (1977).
48. G. Chen, *Phys. Rev. B* 57, 14958 (1998).
49. J. Freund and G. Chen, unpublished.
50. S. M. Lee, D. G. Cahill, and R. Venkatasubramanian, *Appl. Phys. Lett.* 70, 2957 (1997).
51. B. Yang and G. Chen, in "Chemistry, Physics, and Materials Science for Thermoelectric Materials: Beyond Bismuth Telluride" (M. G. Kanatzidis, T. P. Hogan, and S. D. Mahanti, Eds.). Kluwer Academic/Plenum, New York, 2003.
52. G. D. Mahan and M. Bartkowiak, *Appl. Phys. Lett.* 74, 953 (1999).
53. K. H. Yoo and A. C. Anderson, *J. Low Temp. Phys.* 63, 269 (1986).
54. K. Fuchs, *Proc. Cambridge Philos. Soc.* 34, 100 (1938).
55. E. H. Sondheimer, *Phys. Rev.* 80, 401 (1950).

56. C. R. Tellier and A. J. Tosser, "Size Effects in Thin Films." Elsevier, New York, 1982.
57. B. Yang and G. Chen, *Phys. Low-Dimens. Struct.* 5/6, 37 (2000).
58. A. Balandin and K. L. Wang, *Phys. Rev. B.* 58, 1544 (1998).
59. S. Volz and D. Lemonnier, *Phys. Low-Dimens. Struct.* 5/6, 91 (2000).
60. M. Asheghi, M. N. Touzelbaev, K. E. Goodson, Y. K. Leung, and S. S. Wong, *Trans. ASME, J. Heat Transf.* 120, 31 (1998).
61. M. Asheghi, K. Kurabayashi, R. Kasnavi, and K. E. Goodson, *J. Appl. Phys.* 91, 5079 (2002).
62. D. G. Song and G. Chen, in "Proceedings of ICT 2002: 21st International Conference on Thermoelectrics." p. 292, IEEE, New York, 2002.
63. F. Volklein and H. Baltes, *J. Microelectromech. Syst.* 1, 193 (1992).
64. F. Volklein and T. Starz, in "XVI ICT '97: Proceedings of ICT'97, the 16th International Conference on Thermoelectrics," p. 711. IEEE, New York, 1998.
65. Y. C. Tai, C. H. Mastrangelo, and R. S. Muller, *J. Appl. Phys.* 63, 1442 (1988).
66. K. E. Goodson, O. W. Kading, M. Rosner, and R. Zachai, *Appl. Phys. Lett.* 66, 3134 (1995).
67. S. Uma, A. D. McConnell, M. Asheghi, K. Kurabayashi, and K. E. Goodson, *Intl. J. Thermophys.* 22, 605 (2001).
68. A. D. McConnell, S. Uma, and K. E. Goodson, *J. Microelectromech. Syst.* 10, 360 (2001).
69. M. Werner, T. Kohler, S. Mietke, E. Worner, C. Johnston, and H.-J. Fecht, *Proc. SPIE* 4703, 199 (2002).
70. B. C. Daly, H. J. Maris, A. V. Nurmikko, M. Kuball, and J. Han, *J. Appl. Phys.* 92, 3820 (2002).
71. V. Baier, F. Volklein, *Phys. Status Solidi A* 118, K69 (1990).
72. M. Rohde, *Thin Solid Films* 238, 199 (1994).
73. E. J. Gonzalez, J. E. Bonevich, G. R. Stafford, G. White, and D. Josell, *J. Mater. Res.* 15, 764 (2000).
74. S.-M. Lee and D. G. Cahill, *J. Appl. Phys.* 81, 2590 (1997).
75. S.-M. Lee and D. G. Cahill, *Phys. Rev. B* 52, 253 (1995).
76. Y. S. Ju and K. E. Goodson, *J. Appl. Phys.* 85, 7130 (1999).
77. M. B. Kleiner, S. A. Kuhn, and W. Weber, *IEEE Trans. Electron Devices* 43, 1602 (1996).
78. A. J. Griffin, Jr., F. R. Brotzen, and P. L. Loos, *J. Appl. Phys.* 75, 3761 (1994).
79. T. Yao, *Appl. Phys. Lett.* 51, 1298 (1987).
80. W. S. Capinski, H. J. Maris, T. Ruf, M. Cardona, K. Ploog, and D. S. Katzer, *Phys. Rev. B* 59, 8105 (1999).
81. T. Borca-Tasciuc, D. W. Song, J. R. Meyer, I. Vurgaftman, M.-J. Yang, B. Z. Nosho, L. J. Whitman, H. Lee, R. U. Martinelli, G. W. Turner, M. J. Manfra, and G. Chen, *J. Appl. Phys.* 92, 4994 (2002).
82. B. Yang, J. L. Liu, K. L. Wang, and G. Chen, *Appl. Phys. Lett.* 80, 1758 (2002).
83. W. L. Liu, T. Borca-Tasciuc, G. Chen, J. L. Liu, and K. L. Wang, *J. Nanosci. Nanotechnol.* 1, 39 (2001).
84. R. Venkatasubramanian, *Phys. Rev. B* 61, 3091 (2000).
85. T. Borca-Tasciuc, D. Song, J. L. Liu, G. Chen, K. L. Wang, X. Sun, M. S. Dresselhaus, T. Radetic, and R. Gronsky, in "Thermoelectric Materials 1998—Next Generation Materials for Small-Scale Refrigeration and Power Generation Applications. Symposium Proceedings" (T. Tritt, M. G. Kanatzidis, G. D. Mahan, H. B. Lion, Jr., Eds.), Vol. 524, p. 473. Material Research Society, Warrendale, PA, 1999.
86. V. Narayanamurti, *J. Phys. Colloq.* 45, C5/157 (1984).
87. G. Scamarcio, V. Spagnolo, E. Molinari, L. Tapfer, L. Sorba, G. Bratina, and A. Franciosi, *Phys. Rev. B* 46, 7296 (1992).
88. G. Fasol, D. Richards, J. D. White, K. Ploog, C. J. Gibbings, and C. G. Tuppen, *Semicond. Sci. Technol.* 5, 1168 (1990).
89. P. Hyldegaard and G. D. Mahan, *Phys. Rev. B* 56, 10754 (1997).
90. S. Tamura and J. P. Wolfe, *Phys. Rev. B* 38, 5610 (1998).
91. W. E. Bies, R. J. Radtke, and H. Ehrenreich, *J. Appl. Phys.* 88, 1498 (2000).
92. S. Tamura, Y. Tanaka, and H. J. Maris, *Phys. Rev. B* 60, 2627 (1999).
93. G. Chen and M. Neagu, *Appl. Phys. Lett.* 71, 2761 (1997).
94. J. Seyler and M. N. Wybourne, *Phys. Rev. Lett.* 69, 1427 (1992).
95. A. Potts, M. J. Kelly, C. G. Smith, D. G. Hasko, J. R. A. Cleaver, H. Ahmed, D. C. Peacock, J. E. F. Frost, D. A. Ritchie, and G. A. C. Jones, *J. Phys. Condens. Matter* 2, 1817 (1990).
96. A. Potts, M. J. Kelly, D. G. Hasko, J. R. A. Cleaver, H. Ahmed, D. C. Peacock, J. E. F. Frost, D. A. Ritchie, and G. A. C. Jones, *Superlatt. Microstruct.* 9, 315 (1991).
97. A. Potts, M. J. Kelly, D. G. Hasko, J. R. A. Cleaver, H. Ahmed, J. E. F. Frost, D. A. Ritchie, and G. A. C. Jones, *Semicond. Sci. Technol.* 7, B231 (1992).
98. J. Zou and A. Balandin, *J. Appl. Phys.* 89, 2932 (2001).
99. P. Kim, L. Shi, A. Majumdar, and P. L. McEuen, *Phys. Rev. Lett.* 87, 215502 (2001).
100. T. S. Tighe, J. M. Worlock, and M. L. Roukes, *Appl. Phys. Lett.* 70, 2689 (1997).
101. K. Schwab, E. A. Henriksen, J. M. Worlock, and M. L. Roukes, *Nature* 404, 974 (2001).
102. D. E. Angelescu, M. C. Cross, and M. L. Roukes, *Superlatt. Microstruct.* 23, 673 (1998).
103. X. Lü, W. Z. Shen, and J. H. Chu, *J. Appl. Phys.* 91, 1542 (2002).
104. S. Huxtable, D. Li, A. Abramson, A. Miner, W. Kim, M. Chapp, and A. Majumdar, presented at the "US–Japan Nanotherm Seminar: Nanoscale Thermal Science and Engineering," 2002.
105. S. G. Volz and G. Chen, *Appl. Phys. Lett.* 75, 2056 (1999).
106. S. G. Walkauskas, D. A. Broido, K. Kempa, and T. L. Reinecke, *J. Appl. Phys.* 85, 2579 (1999).
107. M. S. Dresselhaus, G. Dresselhaus, and P. C. Eklund, "Science of Fullerenes and Carbon Nanotubes." Academic Press, San Diego, 1996.
108. R. S. Ruoff and D. C. Lorents, *Carbon* 33, 925 (1995).
109. S. Berber, Y.-K. Kwon, and D. Tomanek, *Phys. Rev. Lett.* 84, 4631 (2000).
110. C. Jianwei, T. Cagin, and W. A. Goddard III, *Nanotechnology* 11, 65 (2000).
111. M. A. Osman and D. Srivastava, *Nanotechnology* 12, 21 (2001).
112. J. F. Moreland, J. B. Freund, and G. Chen, *Microscale Thermophys. Eng.*, in press.
113. S. Marayama, *Microscale Thermophys. Eng.* 7, 41 (2003).
114. J. Hone, M. Whitney, C. Piskoti, and A. Zettl, *Phys. Rev. B* 59, R2514 (1999).
115. T. Borca-Tasciuc, C. L. Hapenciuc, B. Wei, R. Vajtai, and P. M. Ajayan, in "Proceedings of the ASME Heat Transfer Division," 2002 (CD-ROM).
116. D. J. Yang, Q. Zhang, G. Chen, S. F. Yoon, J. Ahn, S. G. Wang, Q. Zhou, Q. Wang, and J. Q. Li, *Phys. Rev. B* 66, 165440 (2002).
117. G. Chen, *Trans. ASME, J. Heat Transf.* 118, 539 (1996).
118. G. D. Mahan and F. Claro, *Phys. Rev. B* 38, 1963 (1988).
119. F. Claro and G. D. Mahan, *J. Appl. Phys.* 66, 4213 (1989).
120. P. G. Sverdrup, Y. S. Ju, and K. E. Goodson, *Trans. ASME, J. Heat Transf.* 123, 130 (2001).
121. R. G. Yang, G. Chen, Y. Taur, in "Proceeding of the 12th International Heat Transfer Conference" (J. Taine, Ed.), Vol. 1, pp. 579–584. Elsevier, New York, 2002.
122. Y. Z. Li, L. Vazquez, R. Piner, R. P. Andres, and R. Reifenberger, *Appl. Phys. Lett.* 54, 1424 (1989).
123. P. G. Sverdrup, S. Sinha, S. Uma, M. Asheghi, and K. E. Goodson, *Appl. Phys. Lett.* 78, 3331 (2001).
124. M. I. Kaganov, I. M. Lifshitz, and L. V. Tanatarov, *Zh. Eksp. Teor. Fiz.* 31, 232 (1956) [*Sov. Phys. JETP* 4, 173 (1957)].
125. R. W. Schoenlein, W. Z. Lin, J. G. Fujimoto, and G. L. Easley, *Phys. Rev. Lett.* 58, 1680 (1987).

126. T. Q. Qiu and C. L. Tien, *Trans. ASME, J. Heat Transf.* 115, 835 (1993).
127. K. Banerjee, A. Amerasekera, G. Dixit, N. Cheung, and C. Hu, "International Electron Devices Meeting, Technical Digest," p. 216. IEEE, Piscataway, NJ, 1997.
128. A. Majumdar, K. Fushinobu, and K. Hijikata, *J. Appl. Phys.* 77, 6686 (1995).
129. E. Pop, K. Banerjee, P. Sverdrup, R. Dutton, and K. Goodson, in "International Electron Devices Meeting, Technical Digest," Vol. 951, p. 31.1.1. IEEE, Piscataway, NJ, 2001.
130. G. D. Mahan, *Semicond. Semimetals* 69, p. 172.
131. G. Chen and C. L. Tien, *Trans. ASME, J. Heat Transf.* 114, 636 (1992).
132. K. Richter, G. Chen, and C. L. Tien, *Opt. Eng.* 32, 1897 (1993).
133. P. Y. Wong, C. K. Hess, and I. N. Miaoulis, *Opt. Eng.* 34, 1776 (1995).
134. Z. M. Zhang, B. I. Choi, T. A. Le, M. I. Flik, M. P. Siegal, and J. M. Phillips, *Trans. ASME, J. Heat Transf.* 114, 644 (1992).
135. Z. M. Zhang and M. I. Flik, *IEEE Trans. Appl. Supercond.* 3, 1604 (1993).
136. A. R. Kumar, Z. M. Zhang, V. A. Boychev, D. B. Tanner, L. R. Vale, and D. A. Rudman, *Trans. ASME, J. Heat Transf.* 12, 844 (1999).
137. A. R. Kumar, V. A. Boychev, Z. M. Zhang, and D. B. Tanner, *Trans. ASME, J. Heat Transf.* 122, 785 (2000).
138. C. F. Bohren and D. R. Huffman, "Absorption and Scattering of Light by Small Particles." Wiley, New York, 1983.
139. S. Y. Lin, J. G. Fleming, D. L. Hetherington, B. K. Smith, R. Biswas, K. M. Ho, M. M. Sigalas, W. Zubrzycki, S. R. Kurtz, and J. Bur, *Nature* 394, 251 (1998).
140. G. Subramania, R. Biswas, K. Constant, M. M. Sigalas, K. M. Ho, *Phys. Rev. B* 63, 235111 (2001).
141. A. Rosenberg, R. J. Tonucci, and E. L. Shirley, *J. Appl. Phys.* 82, 6354 (1997).
142. S. D. Hart, G. R. Maskaly, B. Temelkuran, P. H. Prideaux, J. D. Joannopoulos, and Y. Fink, *Science* 296, 510 (2002).
143. C. L. Tien and G. R. Cunnington, *Adv. Heat Transf.* 9, 349 (1973).
144. E. G. Cravolho, C. L. Tien, and R. P. Caren, *Trans. ASME, J. Heat Transf.* 89, 351 (1967).
145. J. B. Pendry, *J. Phys. Condens. Matter* 11, 6621 (1999).
146. C. M. Hargreaves, *Phys. Lett.* 30A, 491 (1969).
147. R. Carminati and J. J. Greffet, *Phys. Rev. Lett.* 82, 1660 (1999).
148. A. V. Shchegrov, K. Joulain, R. Carminati, and J. J. Greffet, *Phys. Rev. Lett.* 85, 1548 (2000).
149. J. Le-Gall, M. Olivier, and J. J. Greffet, *Phys. Rev. B* 55, 10105 (1997).
150. J. P. Mulet, K. Joulain, R. Carminati, and J. J. Greffet, *Appl. Phys. Lett.* 78, 2931 (2001).
151. A. Narayamaswany and G. Chen, *Appl. Phys. Lett.* 82, 3544 (2003).
152. G. A. Domoto and C. L. Tien, *Trans. ASME, J. Heat Transf.* 92, 399 (1970).
153. E. H. Kennard, "Kinetic Theory of Gases." McGraw–Hill, New York, 1938.
154. J. Huisken and E. H. K. Stelzer, *Opt. Lett.* 27, 1223 (2002).
155. J. N. Israelachvili, "Intermolecular and Surface Forces." Academic Press, San Diego/London, 1992.
156. G. E. Karniadakis and A. Beskok, "Micro Flows, Fundamentals and Simmulations." Springer-Verlag, New York, 2001.
157. C.-M. Ho and Y.-C. Tai, *Annu. Rev. Fluid Mech.* 30, 579 (1998).
158. J. C. Maxwell, "A Treatise on Electricity and Magnetism," 2nd ed. Clarendon, Oxford, 1881.
159. J. A. Eastman, S. U. S. Choi, S. Li, W. Yu, and L. J. Thompson, *Appl. Phys. Lett.* 78, 718 (2001).
160. P. Keblinski, S. R. Phillpot, S. U. Choi, and J. A. Eastman, *Int. J. Heat Mass Tranf.* 45, 855 (2002).
161. Y. Taur, C. H. Wann, and D. J. Frank, in "International Electron Devices Meeting 1998, Technical Digest," Vol. 1080, p. 789. IEEE, Piscataway, NJ, 1998.
162. G. Hasnain, K. Tai, L. Yang, Y. H. Wang, R. J. Fischer, J. D. Wynn, B. Weir, N. K. Dutta, and A. Y. Cho, *IEEE J. Quantum Electron.* 27, 1377 (1991).
163. B. Tell, K. F. Brown-Goebeler, and R. E. Leibenguth, *IEEE Photonics Technol. Lett.* 4, 521 (1992).
164. G. Chen, *J. Appl. Phys.* 77, 4152 (1995).
165. H. D. Summers, J. Wu, and J. S. Roberts, *IEE Proc. Optoelectron.* 148, 261 (2001).
166. G. Chen and C. L. Tien, *J. Appl. Phys.* 74, 2167 (1993).
167. J. Tatum, in "2001 IEEE Emerging Technologies Symposium on Broadband Communications for the Internet Era, Symposium Digest" (P. Winson, Ed.), Vol. 161, p. 58. IEEE, Piscataway, NJ, 2001.
168. S. Fukui, and R. Kaneko, *IEEE Trans. Magn.* 24, 2751 (1988).
169. S. Fukui, K. Yamane, and H. Masuda, *IEEE Trans. Magn.* 37, 1845 (2001).
170. E. Grochowski and R. E. Fontana, Jr., in "Seventh Biennial IEEE International Nonvolatile Memory Technology Conference Proceedings," p. 8. IEEE, New York, 1998.
171. S. Sun, C. B. Murray, D. Weller, L. Folks, and A. Moser, *Science* 287, 1989 (2000).
172. W. P. King, T. W. Kenny, K. E. Goodson, G. Cross, M. Despont, U. Durig, H. Rothuizen, G. K. Binnig, and P. Vettiger, *Appl. Phys. Lett.* 78, 1300 (2001).
173. U. Duriga, G. Cross, M. Despont, U. Drechsler, W. Haberle, M. I. Lutwyche, H. Rothuizen, R. Stutz, R. Widmer, P. Vettiger, G. K. Binnig, W. P. King, and K. E. Goodson, *Tribol. Lett.* 9, 25 (2000).
174. A. B. Marchant, "Optical Recording." Addison–Wesley, Reading, MA, 1972.
175. M. Terao, Y. Miyauchi, K. Andoo, H. Yasuoka, and R. Tamura, *Proc. SPIE* 1078, 2 (1989).
176. R. Ito, Y. Tsunoda, H. Ohta, S. Kubota, K. Ogawa, M. Okuda, M. Irie, S. Mitsumori, and H. Nshihara, *Jpn. J. Appl. Phys.* 32, 5185 (1993).
177. H. J. Goldsmid, "Applications of Thermoelectricity." Methuen/Wiley, London/New York, 1960.
178. L. D. Hicks and M. S. Dresselhaus, *Phys. Rev. B* 47, 12727 (1993).
179. T. Koga, X. Sun, S. B. Cronin, M. S. Dresselhaus, K. L. Wang, and G. Chen, *J. Comput.-Aided Mater. Des.* 82, 830 (1997).
180. T. Koga, X. Sun, S. B. Cronin, and M. S. Dresselhaus, *Appl. Phys. Lett.* 75, 2438 (1999).
181. X. Sun, Z. Zhang, and M. S. Dresselhaus, *Appl. Phys. Lett.* 74, 4005 (1999).
182. T. C. Harman, P. J. Taylor, D. L. Spears, and M. P. Walsh, *J. Electron. Mater.* 29, L1 (2000).
183. M. S. Dresselhaus, G. D. Dresselhaus, X. Sun, Z. Zhang, S. B. Cronin, T. Koga, J. Y. Ying, and G. Chen, *Microscale Thermophys. Eng.* 3, 89 (1999).
184. G. Chen, M. S. Dresselhaus, J.-P. Fleurial, and T. Caillat, *Intl. Mat. Rev.* 48, 45 (2003).
185. R. Venkatasubramanian, E. Siivola, T. Colpitts, and B. O'Quinn, *Nature* 413, 597 (2001).
186. T. C. Harman, P. J. Taylor, M. P. Walsh, and B. E. LaForge, *Science* 297, 2229 (2002).
187. J. G. Fleming, S. Y. Lin, I. El-Kady, R. Biswas, and K. M. Ho, *Nature* 417, 52 (2002).
188. M. D. Whale and E. G. Cravalho, *IEEE Trans. Energy Convers.* 17, 130 (2002).
189. M. Kreiter, J. Oster, R. Sambles, S. Herminghaus, S. Mittler-Neher, and W. Knoll, *Opt. Commun.* 168, 117 (1999).
190. B. A. Ridley, B. Nivi, and J. M. Jacobson, *Science* 286, 746 (1999).

191. S. Hector and P. Mangat, *J. Vac. Sci. Technol. B* 19, 2612 (2001).
192. C. Grigoropoulous, in "Proc. DOE 20th Sympos. Energy Eng. Sci.," Argonne, IL, 2002, p. 154.
193. S. Y. Chou, C. Keimel, and J. Gu, *Nature* 417, 835, 2002.
194. Z. F. Ren, Z. P. Huang, J. W. Xu, J. H. Wang, P. Bush, M. P. Siegal, and P. N. Provencio, *Science* 282, 1105 (1998).
195. Y. C. Kong, D. P. Yu, B. Zhang, W. Fang, and S. Q. Feng, *Appl. Phys. Lett.* 78, 407 (2001).
196. Li Mengke, W. Chengwei, and L. Hulin, *Chin. Sci. Bull.* 46, 1793 (2001).
197. D. Routkevitch, A. A. Tager, J. Haruyama, D. Almawlawi, M. Moskovits, and J. M. Xu, *IEEE Trans. Electron Devices* 43, 1646 (1996).
198. Z. Zhang, J. Y. Ying, and M. S. Dresselhaus, *J. Mater. Res.* 13, 1745 (1998).
199. K. Dickmann, J. Jersch, and F. Demming, *Surf. Interface Anal.* 25, 500 (1997).
200. X. Zhang, C. P. Grigoropoulos, D. J. Krajnovich, and A. C. Tam, *IEEE Trans. Compon. Packag. Manuf. Technol. C* 19, 201 (1996).
201. H. J. Mamin and D. Rugar, *Appl. Phys. Lett.* 61, 1003 (1992).
202. K. Hamad-Schifferli, J. J. Schwartz, A. T. Santos. S. Zhang, and J. M. Jacobson, *Nature* 415, 152 (2002).
203. D. G. Cahill, H. E. Fischer, T. Klitsner, E. T. Swartz, and R. O. Pohl, *J. Vac. Sci. Technol. A* 7, 1259 (1989).
204. I. Hatta, *Int. J. Thermophys.* 11, 293 (1990).
205. D. G. Cahill, K. Goodson, and A. Majumdar, *Trans. ASME, J. Heat Transf.* 124, 2 (2002).
206. D. G. Cahil, *Rev. Sci. Instrum.* 61, 802 (1990).
207. T. Borca-Tasciuc, J. L. Liu, T. Zeng, W. L. Liu, D. W. Song, C. D. Moore, G. Chen, K. L. Wang, M. S. Goorsky, T. Radetic, and R. Gronsky, in "Proceedings of the ASME Heat Transfer Division 1999" (L. C. Witte, Ed.), Vol. 364, p. 117. American Society of Mechanical Engineers, New York, 1999.
208. A. R. Kumar, D.-A. Achimov, T. Zeng, and G. Chen, in "Proceedings of the ASME Heat Transfer Division 2000" (J. H. Kim, Ed.), Vol. 366-2, p. 393. American Society of Mechanical Engineers, New York, 2000.
209. T. Borca-Tasciuc, R. Kumar, and G. Chen, *Rev. Sci. Instrum.* 72, 2139 (2001).
210. D. G. Cahill, H. E. Fisher, T. Klitsner, E. T. Swartz, and R. O. Pohl, *J. Vac. Sci. Technol.* 7, 1259 (1989).
211. K. E. Goodson, M. I. Flik, L. T. Su, and D. A. Antoniadis, *Trans. ASME, J. Heat. Transf.* 116, 317 (1994).
212. F. Volklein and J. E. Kessler, *Exp. Tech. Phys.* 33, 343 (1985).
213. P. Nath, K. L. Chopra, *Thin Solid Films* 18, 29 (1973).
214. A. Jacquot, W. L. Liu, G. Chen, J.-P. Fleurial, A. Dauscher, and B. Lenoir, in "Proceedings ICT2002, the 21st Intlernational Conference on Thermoelectrics," p. 353, IEEE, New York, 2002.
215. Z. Zhang and C. P. Grigoropoulos, *Rev. Sci. Instrum.* 66, 115 (1995).
216. T. Borca-Tasciuc, W. L. Liu, J. L. Liu, K. L. Wang, and G. Chen, in "Proceedings of the 2001 National Heat Transfer Conference" (CD-ROM).
217. F. Volklein, *Thin Solids Films* 188, 27 (1990).
218. K. Kurabayashi, M. Asheghi, M. Touzelbaev, and K. E. Goodson, *J. Microelectromech. Syst.* 8, 180, (1999).
219. A. Rosencwaig, J. Opsal, W. L. Smith, and D. L. Weillenborg, *Appl, Phys. Lett.* 46, 1013 (1985).
220. N. M. Amer, M. A. Olmstead, D. Fournier, and A. C. Boccara, *J. Phys. Colloq.* 44, 317 (1983).
221. A. Rosencwaig and A. Gersho, *J. Appl. Phys.* 47, 64 (1976).
222. S. O. Kanstad and P. E. Nordal, *Can. J. Phys.* 64, 1155 (1986).
223. A. C. Boccara, D. Fournier, and J. Badoz, *Appl. Phys. Lett.* 36, 130 (1980).
224. L. Pottier, *Appl. Phys. Lett.* 64, 1618 (1994).
225. J. Hartmann, P. Voigt, and M. Reichling, *J. Appl. Phys.* 81, 2966 (1997).
226. C. A. Paddock and G. Eesley, *J. Appl. Phys.* 60, 285 (1986).
227. K. E. Goodson, O. W. Kading, M. Rosler, and R. Zachai, *J. Appl. Phys.* 77, 1385 (1995).
228. L. J. Inglehart, A. Broniatowski, D. Fournier, A. C. Boccara, and F. Lepoutre, *Appl. Phys. Lett.* 56, 1749 (1990).
229. R. M. Costescu, M. A. Wall, and D. G. Cahill, *Phys. Rev. B* 67, 054302 (2003).
230. O. M. Wilson, X. Hu, D. G. Cahill, and P. V. Braun, *Phys. Rev. B* 66, 224301 (2002).
231. G. Chen, C. L. Tien, X. Wu, and J. S. Smith, *Trans. ASME, J. Heat Transf.* 116, 325 (1994).
232. T. Borca-Tasciuc and G. Chen, *Intl. J. Thermophys.* 19, 557, 1998.
233. D.-A. Borca-Tasciuc, G. Chen, Y. M. Lin, O. Rabin, M. S. Dresselhaus, A. Borshchevsky, J. P. Fleurial, and M. A. Ryan, in "Nanophase and Nanocomposite Materials IV" (S. Komarneni, R. A. Vaia, G. Q. Lu, J.-I. Matsushita, and J. C. Parker, Eds.), Vol. 703, p. V2.7.1-6. Material Research Society, Warrendale, PA, 2001.
234. S. W. Indermuehle and R. B. Peterson, *Trans. ASME, J. Heat Transf.* 121, 528 (1999).
235. L. Shi, Mesoscopic Thermophysical Measurements of Microstructures and Carbon Nanotubes, Ph.D Thesis, University of California at Berkeley, 2001.
236. M. Nonnenmacher and H. K. Wickramasinghe, *Appl. Phys. Lett.* 61, 168 (1992).
237. K. Luo, Z. Shi, J. Varesi, and A. Majumdar, *J. Vac. Sci. Technol. B* 15, 349 (1997).
238. R. J. Pylkki, P. J. Moyer, and P. E. West, *Jpn. J. Appl. Phys. 1* 33, 3785 (1994).
239. M. Maywald, R. J. Pylkki, and L. Balk, *Scanning Microsc.* 8, 181 (1994).
240. A. Majumdar, *Annu. Rev. Mater. Sci.* 29, 505 (1999).
241. E. Betzig and J. K. Trautman, *Science* 257, 189 (1992).
242. B. D. Boudreau, J. Raja, R. J. Hocken, S. R. Patterson, and J. Patten, *Rev. Sci. Instrum.* 68, 3096 (1997).
243. K. E. Goodson and M. Asheghi, *Microscale Thermophys. Eng.* 1, 225 (1997).
244. D. A. Fletcher, K. B. Crozier, C. F. Quate, G. S. Kino, K. E. Goodson, D. Simanovskii, and D. V. Palanker, *Appl. Phys. Lett.* 77, 2109 (2000).
245. A. M. Mansanares, D. Fournier, and A. C. Boccara, *Electron. Lett.* 29, 2045 (1993).
246. J. Christofferson, D. Vashaee, A. Shakouri, and P. Melese, *Proc. SPIE* 4275, 119 (2001).
247. S. Ju, Q. W. Kading, Y. K. Leung, S. S. Wong, and K. E. Goodson, *IEEE Electron Device Lett.* 18, 169 (1997).
248. H. Brugger, P. W. Epperlein, S. Beeck, and G. Abstreiter, in "Proceedings of the 16th International Symposium Gallium Arsenide and Related Compounds Conference" (T. Ikoma and H. Watanabe, Eds.), Vol. 24, p. 771. IOP, Bristol, UK, 1990.
249. R. Puchert, A. Barwolff, U. Menzel, A. Lau, M. Voss, and T. Elsaesser, *J. Appl. Phys.* 80, 5559 (1996).
250. U. Menzel, R. Puchert, A. Barwolff, and A. Lau, *Microelectron. Reliab.* 38, 821 (1998).
251. V. Spagnolo, M. Troccoli, G. Scamarcio, C. Becker, G. Glastre, and C. Sirtori, *Opt. Mater.* 17, 263 (2001).
252. Y. Imry and R. Landauer, *Rev. Mod. Phys.* 71, S306 (1999).
253. M. F. Modest, "Radiative Heat Transfer." McGraw–Hill, New York, 1993.
254. D. K. Ferry, "Semiconductors." MacMillan Co., New York, 1991.
255. J. Callaway, *Phys. Rev.* 113, 1046 (1959).
256. C. Cercignani, "Rarefied Gas Dynamics: From Basic Concepts to Actual Calculations." Cambridge, New York, 2000.
257. H. B. Casimir, *Physica* 5, 495 (1938).
258. F. Volklein and E. Kessler, *Thin Solid Films* 142, 169 (1986).
259. U. Dilliner and F. Volklein, *Thin Solid Films* 187, 263 (1990).

260. G. Chen and C. L. Tien, *AIAA J. Thermophys. Heat Transf.* 7, 311 (1993).
261. S. Kumar, G. C. Vradis, *Trans. ASME, J. Heat Transf.* 116, 28 (1994).
262. M. I. Flik and C. L. Tien, *Trans. ASME, J. Heat Transf.* 112, 872 (1990).
263. A. Majumdar, *Trans. ASME, J. Heat Transf.* 115, 7 (1993).
264. C. P. Jen and C. C. Chieng, *J. Thermophys. Heat Transf.* 12, 146 (1998).
265. T. Zeng and G. Chen, *Trans. ASME, J. Heat Transf.* 123, 340 (2001).
266. X. Y. Yu, G. Chen, A. Verma, and J. S. Smith, *Appl. Phys. Lett.* 67, 3554 (1995).
267. C. K. Chan and C. L. Tien, *Trans. ASME, J. Heat Transf.* 95, 302 (1973).
268. D. W. Song, W.-N. Shen, T. Zeng, W. L. Liu, G. Chen, B. Dunn, C. D. Moore, M. S. Goorsky, R. Radetic, and R. Gronsky, in "Proceedings of the ASME Heat Transfer Division 1999" (L. C. Witte, Ed.). American Society of Mechanical Engineers, New York, 1999.
269. G. Gesele, J. Linsmeier, V. Drach, J. Fricke, and R. Arens-Fischer, *J. Phys. D* 30, 2911 (1997).
270. V. Lysenko, V., Gliba, V. Strikha, A. Dittmar, G. Delhomme, Ph. Roussell, D. Barbier, N. Jaffrezic, and C. Martelet, *Appl. Surf. Sci.* 123, 458 (1998).
271. J. D. Chung and M. Kaviany, *Int. J. Heat Mass Tranf.* 43, 521 (2000).
272. J. O. Sofo and G. D. Mahan, in "18th International Conference on Thermoelectrics: Proceedings, ICT'99," Vol. 736, p. 626. IEEE, Piscataway, NJ, 1999.
273. Ce-Wen Nan, R. Birringer, David R. Clarke, and H. Gleiter, *J. Appl. Phys.* 81, 6692 (1997).
274. O. Tornblad, P. G. Sverdrup, D. Yergeau, Z. Yu, K. E. Goodson, and D. W. Dutton, in "2000 International Conference on Simulation Semiconductor Processes and Devices," Vol. 282, p. 58. IEEE, Piscataway, NJ, 2002.
275. J. R. Howell, *J. Heat Transf.* 120, 547 (1998).
276. C. Moglestue, *Comput. Methods Appl. Mech. Eng.* 30, 173 (1982).
277. C. Jacoboni and L. Reggiani, *Rev. Mod. Phys.* 55, 645 (1983).
278. M. V. Fischetti and S. E. Laux, *Phys. Rev. B* 38, 9721 (1988).
279. M. V. Fischetti and S. E. Laux, *Phys. Rev. B* 48, 2244 (1993).
280. P. Lugli, P. Bordone, L. Reggiani, M. Rieger, P. Kocevar, and S. M. Goodnick, *Phys. Rev. B* 39, 7852 (1989).
281. R. B. Peterson, *Trans. ASME, J. Heat Transf.* 16, 815 (1994).
282. T. Klitsner, J. E. VanCleve, H. E. Fischer, and R. O. Pohl, *Phys. Rev. B* 38, 7576 (1988).
283. S. Mazumder and A. Majumdar, *Trans. ASME, J. Heat Transf.* 123, 749 (2001).
284. R. L. Liboff, "Kinetic Theory." Prentice Hall, Englewood Cliffs, NJ, 1998.
285. G. D. Mahan, "Many-Particle Physics." Kluwer Academic/Plenum P. New York, 2000.
286. Z. B. Zhang, M. S. Dresselhaus, and J. Y. Ying, *Mater. Res. Soc. Symp. Proc.* 524, 351 (1999).
287. Y. M. Lin, S. B. Cronin, J. Y. Ying, J. Heremans, and M. S. Dresselhaus, in *Mater. Res. Soc. Symp. Proc.* 635, C4.30.1 (2001).
288. J. L. Liu, J. Wan, Z. M. Jiang, A. Khitun, K. L. Wang, and D. P. Yu, *J. Appl. Phys.* 92, 6804 (2002).
289. B. Pendry, "Low Energy Electron Diffraction." Academic Press, New York, 1974.
290. M. V. Simkin and G. D. Mahan, *Phys. Rev. Lett.* 84, 927 (2000).
291. B. Yang and G. Chen, in "Proceedings ICT2002: 21st International Conference on Thermoelectrics," p. 306, IEEE, New York, 2002.
292. D. Frenkel and B. Smit, "Understanding Molecular Simulation, From Algorithm to Applications." Academic Press, London, 1996.
293. D. C. Rapaport, "The Art of Molecular Dynamics." Cambridge Univ. Press, Cambridge, UK, 1995.
294. J. P. Hansen and I. A. MacDonald, "Theory of Simple Liquids." Academic Press, New York, 1990.
295. Q. M. Yu, M. O. Thompson, and P. Clancy, *Phys. Rev. B* 53, 8386 (1996).
296. S. Kotake and S. Wakuri, *JSME Int. J. B* 37, 103 (1994).
297. S. Volz, J. B. Saulnier, M. Lallemand, B. Perrin, P. Depondt, and M. Mareschal, *Phys. Rev. B* 54, 340 (1996).
298. R. D. Mountain and R. A. MacDonald, *Phys. Rev. B* 28, 3022 (1983).
299. A. Tenenbaum, G. Ciccotti, and R. Gallico, *Phys. Rev. A* 25, 2778 (1982).
300. R. H. H. Poetzsch and H. Boettger, *Phys. Rev. B* 50, 15757 (1994).
301. S. Volz and G. Chen, *Phys. Rev. B* 61, 2651 (2000).
302. A. J. C. Ladd, B. Moran, and W. G. Hoover, *Phys. Rev. B* 34, 5058 (1986).
303. J. Che, T. Cagin, W. Deng, and W. A. Goddard III, *J. Chem. Phys.* 113, 6888 (2000).
304. J. R. Lukes, D. Y. Li, X. G. Liang, and C. L. Tien, *Trans. ASME, J. Heat Transf.* 122, 536 (2000).
305. L. J. Porter, J Li, and S. Yip, *J. Nucl. Mater.* 246, 53 (1997).
306. J. Li, L. J. Porter, and S. Yip, *J. Nucl. Mater.* 255, 139 (1998).
307. F. H. Stillinger and T. A. Webber, *Phys. Rev. B* 31, 5262 (1985).
308. M. Moseler and U. Landman, *Science* 289, 1165 (2000).
309. A. Nakano, M. E. Bachlechner, P. Branicio, T. J. Campbell, I. Ebbsjo, R. K. Kalia, A. Madhukar, S. Ogata, A. Omeltchenko, J. P. Rino, F. Shimojo, P. Walsh, and P. Vashishta *IEEE Trans. Electron Devices* 47, 1804 (2000).
310. T. Ikeshoji and B. Hafskjold, *Mol. Phys.* 81, 251 (1994).
311. F. Muller-Plathe, *J. Chem. Phys.* 106, 6082 (1997).
312. J. R. Lukes, D. Y. Li, X. G. Liang, and C. L. Tien, *Trans. ASME, J. Heat Transf.* 122, 536 (2000).
313. R. Kubo, *J. Phys. Soc. Jpn.* 12, 570 (1957).
314. R. Kubo and M. Yokota, *J. Phys. Soc. Jpn.* 12, 1203 (1957).
315. R. Zwanzig, *Anna. Rev. Phys. Chem.* 16, 67 (1964).
316. S. Volz, J. B. Saulnier, G. Chen, and P. Beauchamp, *High Temp.–High Press.* 32, 709 (2000).
317. X. G. Liang and B. Shi, *Mater. Sci. Eng. A* 292, 198 (2000).
318. P. Chantrenne and M. Raynaud, in "Proceedings of the 12th International Heat Transfer Conference" (J. Taine, Ed.), Vol. 1, p. 549. Elsevier, New York, 2002.
319. A. R. Abramson, C.-L. Tien, and A. Majumdar, *Trans. ASME, J. Heat Transf.* 124, 963 (2002).
320. Chen, Voltz, and Freund, private communication.
321. R. J. Stoner and H. J. Maris, *Phys. Rev. B* 48, 16373 (1993).
322. M. E. Lumpkin and W. M. Saslow, *Phys. Rev. B* 20, 1035 (1979).
323. Y. Ge and S. Chen, *Solid State Commun.* 77, 313 (1991).
324. A. Maiti, G. D. Mahan, and S. T. Pantelides, *Solid State Commun.* 102, 517 (1997).
325. S. M. Rytov, Theory of Electric Fluctuations and Thermal Radiation, AFCRC-TR-59-162, Air Force Cambridge Research Center, Bedford, MA, 1959.
326. G. Chen, *Microscale Thermophys. Eng.* 1, 215 (1997).
327. L. M. Phinney and C. L. Tien, *Trans. ASME, J. Heat Transf.* 3, 751 (1998).
328. K. Blotekjaer, *IEEE Trans. Electron Devices* 17, 38 (1970).
329. K. A. Fushinobu, A. Majumdar, and K. Hijikata, *Trans. ASME, J. Heat Transf.* 117, 25 (1995).
330. A. Majumdar, K. A. Fushinobu, and K. Hijikata, *J. Appl. Phys.* 77, 6686 (1995).
331. J. Lai and A. Majumdar, *Appl. Phys.* 79, 7353 (1996).
332. T. Q. Qiu and C. L. Tien, *Int. J. Heat Mass Transf.* 37, 2799 (1994).
333. M. Lundstrom, "Fundamentals of Carrier Transport," 2nd ed. Cambridge Univ. Press, Cambridge, UK, 2000.

334. H. J. Goldsmid, "Thermoelectric Rrefrigeration." Plenum Press, New York, 1964.
335. L. P. Bulat and V. G. Yatsyuk, *Sov. Phys.-Semicond.* 18, 383 (1984).
336. L. I. Anatychuk, L. P. Bulat, D. D. Nikirsa, and V. G. Yatsyuk, *Sov. Phys.-Semicond.* 21, 206 (1987).
337. G. Chen, *Int. J. Therm. Sci.* 40, 693 (2001).
338. R. G. Yang and G. Chen, in "Proceedings of the International Mechanical Engineering Conference and Exhibitions," 2001 (CD-ROM).
339. S. V. J. Narumanchi, J. Murthy, and C. H. Amon, in "Proceedings of the International Mechanical Engineering Conference and Exhibitions," 2001 (CD-ROM).
340. G. Chen, *Appl. Phys. Lett.* 82, 991 (2003).